

1 Dear Editor and Reviewers,
2

3 We thank the reviewers and executive editor for their constructive suggestions and comments on
4 our manuscript. Below is a point-by-point response to all reviewer and editor comments.
5

6 Many thanks,
7

8 Chris Reinhard (on behalf of all coauthors)
9
10
11

12 EXECUTIVE EDITOR COMMENTS:
13

14 In particular, please note that for your paper, the following requirement has not been met in the
15 Discussions paper:
16

17 • "The main paper must give the model name and version number (or other unique identifier) in
18 the title."
19

20 Please add a version number (the Github TAG number) for cGENIE in the title upon your
21 revised submission to GMD.
22

23 -This information has now been added to the title.
24

25 REVIEWER #1
26

27 The kinetics of CH₄ degradation are described as an O₂-O₃-CH₄ parameterization, but there is
28 no mention of O₃ except for that. Does O₃ do anything interesting at different O₂
29 concentrations, or during the CH₄ spike? If not, it would still be worth a sentence describing
30 what role O₃ is playing in the parameterization, just for clarity.
31

32 -This is a good point. We have added the following text to clarify: "We note that in this
33 parameterization, O₃ abundance is not calculated explicitly, but rather the photochemical
34 destruction rate of CH₄ in the atmosphere is implicitly controlled by the combined atmospheric
35 chemistry embedded within keff."
36
37

38 On line 601 it is suggested that CH₄ warming might explain the warmth of the PETM. This was
39 what Schmidt and Shindell assumed, but it doesn't work because the warming persisted after the
40 release period was over, meaning that it must have been CO₂, not CH₄.
41

42 -We certainly do not mean to suggest that the temperature changes observed during the course of
43 the PETM are entirely attributable to changes in CH₄ cycling. The time-dependent analysis is
44 only meant to illustrate the transient behavior of the model during an idealized perturbation,
45 rather than to evaluate any particular scenario for explaining previous climate transients in
46 Earth's history. We have added the following clause to this portion of the text in order to

47 emphasize this (Line 573): "This is meant only to illustrate the time-dependent behavior of the
48 model in the face of an idealized carbon cycle perturbation, rather than to evaluate any particular
49 scenario for explaining previous climate transients in Earth's history."
50

51
52

53 REVIEWER #2

54

55 478: Restructure The subject of this sentence should be 'metabolic fluxes' not 'Figure 6'

56

57 -This has been changed.

58

59

60 547: Again, making the Figure lead the science, rather than vice versa.

61

62 -This has been changed.

63

64

65 558: suggest rephrasing for international audiences 'effective throttle'

66

67 -This has been changed to: "...AOM dominates the consumption of CH₄ produced in the ocean
68 interior and is extremely effective at reducing CH₄ fluxes to the atmosphere."
69

70

71

72 646: Avoid telling the reader that they should find something 'interesting'.

73

74 -We have removed "Interestingly, ..." from the beginning of the sentence.

75

76

77

78

79

80

81

82

83

84

85

86

87

88

89

90

91

92

93 **Oceanic and atmospheric methane cycling in the cGENIE Earth system model –**
94 **release v0.9.14**

95
96 Christopher T. Reinhard^{1,2,3*}, Stephanie L. Olson^{2,4,5}, Sandra Kirtland Turner⁶, Cecily Pálíke⁷, Yoshiki Kanzaki⁶,
97 Andy Ridgwell⁶

98
99 ¹School of Earth and Atmospheric Sciences, Georgia Institute of Technology, Atlanta, GA 30332

100 ²NASA Astrobiology Institute, Alternative Earths Team, Riverside, CA

101 ³NASA Nexus for Exoplanet System Science (NExSS) Upside-Down Biospheres Team, Georgia Institute of
102 Technology, Atlanta, GA

103 ⁴Department of Geophysical Sciences, University of Chicago, Chicago, IL 60637

104 ⁵Department of Earth, Atmospheric, and Planetary Science, Purdue University, West Lafayette, IN 47907

105 ⁶Department of Earth and Planetary Sciences, University of California, Riverside, Riverside, CA 92521

106 ⁷MARUM Center for Marine Environmental Sciences, University of Bremen, Germany

107
108 *To whom correspondence should be addressed. E-mail: chris.reinhard@cas.gatech.edu
109

110 **Abstract: The methane (CH₄) cycle is a key component of the Earth system that links**
111 **planetary climate, biological metabolism, and the global biogeochemical cycles of carbon,**
112 **oxygen, sulfur, and hydrogen. However, currently lacking is a numerical model capable of**
113 **simulating a diversity of environments in the ocean where CH₄ can be produced and**
114 **destroyed, and with the flexibility to be able to explore not only relatively recent**
115 **perturbations to Earth’s CH₄ cycle but also to probe CH₄ cycling and associated climate**
116 **impacts under the very low-O₂ conditions characteristic of most of Earth history and likely**
117 **widespread on other Earth-like planets. Here, we present a refinement and expansion of the**
118 **ocean-atmosphere CH₄ cycle in the intermediate-complexity Earth system model cGENIE,**
119 **including parameterized atmospheric O₂-O₃-CH₄ photochemistry and schemes for microbial**
120 **methanogenesis, aerobic methanotrophy, and anaerobic oxidation of methane (AOM). We**
121 **describe the model framework, compare model parameterizations against modern**
122 **observations, and illustrate the flexibility of the model through a series of example**
123 **simulations. Though we make no attempt to rigorously tune default model parameters, we**
124 **find that simulated atmospheric CH₄ levels and marine dissolved CH₄ distributions are**
125 **generally in good agreement with empirical constraints for the modern and recent Earth.**
126 **Finally, we illustrate the model’s utility in understanding the time-dependent behavior of the**
127 **CH₄ cycle resulting from transient carbon injection into the atmosphere, and present model**
128 **ensembles that examine the effects of atmospheric pO₂, oceanic dissolved SO₄²⁻, and the**
129 **thermodynamics of microbial metabolism on steady-state atmospheric CH₄ abundance.**
130 **Future model developments will address the sources and sinks of CH₄ associated with the**
131 **terrestrial biosphere and marine CH₄ gas hydrates, both of which will be essential for**
132 **comprehensive treatment of Earth’s CH₄ cycle during geologically recent time periods.**
133

134 **1. Introduction**

135 The global biogeochemical cycle of methane (CH₄) is central to the evolution and climatic stability
136 of the Earth system. Methane provides an important substrate for microbial metabolism,
137 particularly in energy-limited microbial ecosystems in the deep subsurface (Valentine,
138 2011;Chapelle et al., 1995) and in anoxic marine and lacustrine sediments (Lovley et al.,

139 1982;Hoehler et al., 2001). Indeed, the microbial production and consumption of CH₄ are amongst
140 the oldest metabolisms on Earth, with an isotopic record of bacterial methane cycling stretching
141 back nearly 3.5 billion years (Ueno et al., 2006;Hinrichs, 2002;Hayes, 1994). As the most abundant
142 hydrocarbon in Earth's atmosphere CH₄ also has a significant influence on atmospheric
143 photochemistry (Thompson and Cicerone, 1986), and because it absorbs in a window region of
144 Earth's longwave emission spectrum it is an important greenhouse gas. This has important
145 implications over the coming centuries, with atmospheric CH₄ classified as a critical near-term
146 climate forcing (Myhre et al., 2013), but has also resulted in dramatic impacts during certain
147 periods of Earth history. For example, high steady-state atmospheric CH₄ has been invoked as an
148 important component of Earth's early energy budget, potentially helping to offset a dim early Sun
149 (Sagan and Mullen, 1972;Pavlov et al., 2000;Haqq-Misra et al., 2008), while time-dependent
150 changes to the atmospheric CH₄ inventory have been invoked as drivers of extreme climatic
151 perturbations throughout Earth history (Dickens et al., 1997;Dickens, 2003;Bjerrum and Canfield,
152 2011;Zeebe, 2013;Schrag et al., 2002). Because it is cycled largely through biological processes
153 on the modern (and ancient) Earth and is spectrally active, atmospheric CH₄ has also been
154 suggested as a remotely detectable biosignature that could be applied to planets beyond our solar
155 system (Hitchcock and Lovelock, 1967;Sagan et al., 1993;Krissansen-Totton et al., 2018).

156
157 A number of low-order Earth system models incorporating a basic CH₄ cycle have been developed,
158 particularly with a view to addressing relatively 'deep time' geological questions. These include
159 explorations of long-term changes to the chemistry of Earth's atmosphere (Claire et al.,
160 2006;Catling et al., 2007;Bartdorff et al., 2008;Beerling et al., 2009), potential climate impacts at
161 steady state (Kasting et al., 2001;Ozaki et al., 2018), and transient impacts of CH₄ degassing on
162 climate (Schrag et al., 2002;Bjerrum and Canfield, 2011). In some cases these models explicitly
163 couple surface fluxes to a model of atmospheric photochemistry (Lamarque et al., 2006;Ozaki et
164 al., 2018;Kasting et al., 2001), but in general atmospheric chemistry is parameterized based on
165 offline 1- or 2-D photochemical models while surface fluxes are specified arbitrarily or are based
166 on a simple 1-box ocean-biosphere model. A range of slightly more complex 'box' model
167 approaches have been applied to simulate transient perturbations to Earth's CH₄ cycle and
168 attendant climate impacts on timescales ranging from ~10⁵ years (Dickens et al., 1997;Dickens,
169 2003) to ~10⁸ years (Daines and Lenton, 2016). In addition, offline and/or highly parameterized

170 approaches toward simulating the impact of transient CH₄ degassing from gas hydrate reservoirs
171 have been developed and applied to relatively recent periods of Earth history (Archer and Buffett,
172 2005;Lunt et al., 2011) or projected future changes (Archer et al., 2009;Hunter et al., 2013).
173 However, the most sophisticated and mechanistic models of global CH₄ cycling currently available
174 tend to focus on terrestrial (soil or wetland) sources and sinks (Ridgwell et al., 1999;Walter and
175 Heimann, 2000;Wania et al., 2010;Konijnendijk et al., 2011;Melton et al., 2013) or focus on
176 explicitly modeling atmospheric photochemistry (Shindell et al., 2013).

177

178 Much less work has been done to develop ocean biogeochemistry models that are both equipped
179 to deal with the wide range of boundary conditions characteristic of Earth history and are
180 computationally tractable when running large model ensembles and/or on long (approaching ~10⁶
181 year) timescales, as well as being able to simulate the (3-D) redox structure of the ocean allowing
182 for localized zones of production and oxidation (which provides more accurate estimates of
183 emission to the atmosphere). For instance, Elliot et al. (2011) advanced modelling of marine CH₄
184 cycling by developing and employing a 3-D ocean circulation and climate model (CCSM-3) to
185 simulate the impact of injecting clathrate-derived CH₄ into the Arctic ocean. However, microbial
186 consumption of CH₄ in the ocean interior was parameterized via an empirical log-linear function
187 that implicitly neglects anaerobic oxidation of methane (AOM) via dissolved sulfate (SO₄²⁻), which
188 on the modern Earth is an enormously important internal CH₄ sink within Earth's oceans (Egger
189 et al., 2018). Their simulations did not explore atmospheric chemistry. Similarly, Daines and
190 Lenton (2016) also innovated over traditional box modelling approaches by applying an ocean
191 general circulation model (GCM) to examine the role of aerobic methanotrophy in modulating
192 ocean-atmosphere fluxes of CH₄ during Archean time (prior to ~2.5 billion years ago, Ga).
193 However, this analysis likewise did not include AOM, and the GCM results were not coupled to
194 atmospheric chemistry. In contrast, Olson et al. (2016) included AOM in a 3-D ocean
195 biogeochemistry model coupled to an atmospheric chemistry routine and found that AOM
196 represents a critical internal CH₄ sink in the oceans even at relatively low dissolved SO₄²⁻ levels.
197 Though this represented an important further step forward in understanding marine CH₄ cycling
198 on the early Earth, Olson et al. (2016) employed a simplified parameterization of aerobic CH₄
199 consumption, neglected the thermodynamics of CH₄-consuming metabolisms under energy-
200 limited conditions, and employed a parameterization of atmospheric O₂-O₃-CH₄ photochemistry

201 that is most readily applicable to only a subset of the atmospheric pO_2 values characteristic of
202 Earth history (Daines and Lenton, 2016;Olson et al., 2016). While all of these studies provided
203 new modelling innovations and advances in understanding, important facets of global CH_4 cycling,
204 particularly as relevant to the evolution of early Earth, were lacking.

205

206 Here, we present a new framework for modeling the ocean-atmosphere biogeochemical CH_4 cycle
207 in the ‘muffin’ release of the cGENIE Earth system model. Our goal is to make further progress
208 in the development of a flexible intermediate-complexity model suitable for simulating the global
209 biogeochemical CH_4 cycle on ocean-bearing planets, with an initial focus on periods of Earth
210 history (or other habitable ocean-bearing planets) that lack a robust terrestrial biosphere. We also
211 aim to provide a numerical modeling foundation from which to further develop a more complete
212 CH_4 cycle within the cGENIE framework, including, for example, dynamic CH_4 hydrate cycling
213 and the production/consumption of CH_4 by terrestrial ecosystems.

214

215 The outline of the paper is as follows. In Section 2 we briefly describe the GENIE/cGENIE Earth
216 system model, with a particular eye toward the features that are most relevant for the biological
217 carbon pump and the oceanic CH_4 cycle. In Section 3 we describe the major microbial metabolisms
218 involved in the oceanic CH_4 cycle and compare our parameterizations to data from modern marine
219 environments. In Section 4 we describe two alternative parameterizations of atmospheric O_2 - O_3 -
220 CH_4 photochemistry incorporated into the model and compare these to modern/recent
221 observations. In Section 5 we present results from a series of idealized simulations meant to
222 illustrate the flexibility of the model and some potential applications. The availability of the model
223 code, plus configuration files for all experiments described in the paper, is provided in Section 7,
224 following a brief summary in Section 6.

225

226 **2. The GENIE/cGENIE Earth system model**

227 **2.1. Ocean physics and climate model – C-GOLDSTEIN**

228 The ocean physics and climate model in cGENIE is comprised of a reduced physics (frictional
229 geostrophic) 3-D ocean circulation model coupled to both a 2-D energy-moisture balance model
230 (EMBM) and a dynamic-thermodynamic sea-ice model (Edwards and Marsh, 2005;Marsh et al.,
231 2011). The ocean model transports heat, salinity, and biogeochemical tracers using a scheme of

232 parameterized isoneutral diffusion and eddy-induced advection (Griffies, 1998;Edwards and
233 Marsh, 2005;Marsh et al., 2011), exchanges heat and moisture with the atmosphere, sea ice, and
234 land, and is forced at the ocean surface by the input of zonal and meridional wind stress according
235 to a specified wind field. The 2-D atmospheric energy-moisture-balance model (EMBM) considers
236 the heat and moisture balance for the atmospheric boundary layer using air temperature and
237 specific humidity as prognostic tracers. Heat and moisture are mixed horizontally throughout the
238 atmosphere, and exchange heat and moisture with the ocean and land surfaces with precipitation
239 occurring above a given relative humidity threshold. The sea-ice model tracks the horizontal
240 transport of sea ice, and the exchange of heat and freshwater with the ocean and atmosphere using
241 ice thickness, areal fraction, and concentration as prognostic variables. Full descriptions of the
242 model and coupling procedure can be found in Edwards and Marsh (2005) and, more recently, in
243 Marsh et al. (2011). As implemented here, the ocean model is configured as a 36 x 36 equal-area
244 grid (uniform in longitude and uniform in the sine of latitude) with 16 logarithmically spaced depth
245 levels and seasonal surface forcing from the EMBM.

246

247 **2.2. Ocean biological pump – BIOGEM**

248 The biogeochemical model component — ‘BIOGEM’ — regulates air-sea gas exchange as well
249 as the transformation and partitioning of biogeochemical tracers within the ocean, as described in
250 Ridgwell et al. (2007). By default, the biological pump is driven by parameterized uptake of
251 nutrients in the surface ocean, with this flux converted stoichiometrically to biomass that is then
252 partitioned into either dissolved or particulate organic matter for downstream transport, sinking,
253 and remineralization. Dissolved organic matter is transported by the ocean model and decays with
254 a specified time constant, while particulate organic matter is immediately exported out of the
255 surface ocean and partitioned into two fractions of differing lability. In the ocean interior,
256 particulate organic matter is remineralized instantaneously throughout the water column following
257 an exponential decay function with a specified remineralization length scale.

258

259 In the simulations discussed below, photosynthetic nutrient uptake in surface ocean grid cells is
260 controlled by a single limiting nutrient, dissolved phosphate (PO_4):

$$\frac{\partial \text{PO}_4}{\partial t} = -\Gamma + \lambda \text{DOP}, \quad (1)$$

$$\frac{\partial \text{DOP}}{\partial t} = \nu \Gamma - \lambda \text{DOP}, \quad (2)$$

261 where DOP represents dissolved organic phosphorus, ν represents the proportion of photosynthetic
 262 production that is initially partitioned into a dissolved organic phase, λ represents a decay constant
 263 (time⁻¹) for dissolved organic matter, and Γ represents photosynthetic nutrient uptake following
 264 Doney et al. (2006):

$$\Gamma = F_I \cdot F_N \cdot F_T \cdot (1 - f_{ice}) \cdot \frac{[\text{PO}_4]}{\tau_{bio}}. \quad (3)$$

265 Rates of photosynthesis are regulated by terms describing the impact of available light (F_I),
 266 nutrient abundance (F_N), temperature (F_T), and fractional sea ice coverage in each grid cell (f_{ice}).
 267 Rates of photosynthetic nutrient uptake are further scaled to ambient dissolved PO₄ ([PO₄])
 268 according to an optimal uptake timescale (τ_{bio}).

269

270 Note that this parameterization differs from that in Ridgwell et al. (2007). Specifically, the impacts
 271 of light and nutrient availability are both described via Michaelis-Menten terms:

$$F_I = \frac{I}{I + \kappa_I}, \quad (4)$$

$$F_N = \frac{[\text{PO}_4^3]}{\kappa_P + [\text{PO}_4^3]}, \quad (5)$$

272 where shortwave irradiance I is averaged over the entire mixed layer, and is assumed to decay
 273 exponentially from the sea surface with a length scale of 20 m. It is assumed that nutrient uptake
 274 and photosynthetic production only occur in surface grid cells of cGENIE (e.g., the upper 80 m),
 275 which is similar to the ‘compensation depth’ z_c in Doney et al. (2006) of 75 m. The terms κ_I and
 276 κ_P represent half-saturation constants for light and dissolved phosphate, respectively. In addition,
 277 the effect of temperature on nutrient uptake is parameterized according to:

$$F_T = k_{T0} \cdot \exp\left[\frac{T}{k_{eT}}\right], \quad (6)$$

278 where k_{T0} and k_{eT} denote pre-exponential and exponential scaling constants and T represents
 279 absolute *in-situ* temperature. The scaling constants are chosen to give approximately a factor of
 280 two change in rate with a temperature change of 10°C (e.g., a Q₁₀ response of ~2.0). Lastly, the

281 final term in Eq. (3), not present in the default parameterization of Ridgwell et al. (2007), allows
 282 for biological productivity to scale more directly with available PO₄ when dissolved PO₄
 283 concentrations are elevated relative to those of the modern oceans.

284

285 Particulate organic matter (POM) is immediately exported out of the surface ocean without lateral
 286 advection, and is instantaneously remineralized throughout the water column according to an
 287 exponential function of depth:

$$F_z^{POM} = F_{z=z_h}^{POM} \cdot \left(\sum_i r_i^{POM} \cdot \exp\left(\frac{z_h - z}{l_i^{POM}}\right) \right), \quad (7)$$

288 where F_z^{POM} is the particulate organic matter flux at a given depth (and z_h is the base of the photic
 289 zone), z is depth, r_i^{POM} and l_i^{POM} refer to the relative partitioning into each organic matter lability
 290 fraction i and the e -folding depth of that fraction, respectively. The simulations presented here
 291 employ two organic matter fractions, a ‘labile’ fraction (94.5%) with an e -folding depth of ~590
 292 m and an effectively inaccessible fraction (5.5%) with an e -folding depth of 10⁶ m (**Table 1**).

293

294 We employ a revised scheme for organic matter remineralization in the ocean interior, following
 295 that commonly used in models of organic matter remineralization within marine and lacustrine
 296 sediments (Rabouille and Gaillard, 1991; Van Cappellen et al., 1993; Boudreau, 1996a, b).
 297 Respiratory electron acceptors (O₂, NO₃⁻, and SO₄²⁻) are consumed according to decreasing free
 298 energy yield (Froelich et al., 1979), with consumption rates (R_i) scaled to both electron acceptor
 299 abundance and the inhibitory impact of electron acceptors with higher intrinsic free energy yield:

$$R_{O_2} = \frac{[O_2]}{\kappa_{O_2} + [O_2]}, \quad (8)$$

$$R_{NO_3} = \frac{[NO_3]}{\kappa_{NO_3} + [NO_3]} \cdot \frac{\kappa_{O_2}^i}{\kappa_{O_2}^i + [O_2]}, \quad (9)$$

$$R_{SO_4} = \frac{[SO_4]}{\kappa_{SO_4} + [SO_4]} \cdot \frac{\kappa_{O_2}^i}{\kappa_{O_2}^i + [O_2]} \cdot \frac{\kappa_{NO_3}^i}{\kappa_{NO_3}^i + [NO_3]}, \quad (10)$$

300 with the exception that in the biogeochemical configuration used here we do not consider nitrate
 301 (NO₃⁻). The total consumption of settling POM within each ocean layer is governed by the
 302 predetermined remineralization profiles (Equation 7). The R_i terms denote the relative fraction of

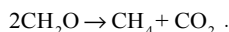
303 this organic matter consumption that is performed by each respiratory process. We specify a closed
304 system with no net organic matter burial in marine sediments (see below) and hence the POM flux
305 to the sediment surface is assumed to be completely degraded, with the same partitioning amongst
306 electron acceptors carried out according to local bottom water chemistry. For DOM, the assumed
307 lifetime (λ) determines the total fraction of DOM degraded (and Equations 8-10 again determine
308 how the consumption of electron acceptors is partitioned). The κ_i terms represent half-saturation
309 constants for each metabolism, κ_i^j terms give inhibition constants acting on less energetic
310 downstream respiratory processes, and brackets denote concentration. Default parameter values
311 used here are shown in **Table 1**.

312

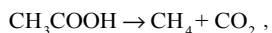
313 **3. Oceanic methane cycling**

314 **3.1. Microbial methanogenesis**

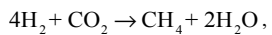
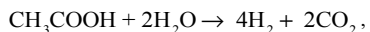
315 Methanogenesis represents the terminal step in our remineralization scheme, and follows the
316 overall stoichiometry:



317 This can be taken to implicitly include fermentation of organic matter to acetate followed by
318 acetoclastic methanogenesis:



319 or the fermentation of organic matter to acetate followed by anaerobic acetate oxidation and
320 hydrogenotrophic methanogenesis:



321 both of which have the same overall net stoichiometry provided that H_2 is assumed to be
322 quantitatively converted to CH_4 by hydrogenotrophic methanogens. We thus ignore the scenario
323 in which some fraction of H_2 is converted directly to biomass by hydrogenotrophic methanogens
324 acting as primary producers (Ozaki et al., 2018).

325

326 Because we specify a closed system with no net organic matter burial in marine sediments, all
 327 organic matter not remineralized by more energetic respiratory metabolisms is converted into CH₄
 328 (e.g., $R_{CH_4} = 1 - R_{O_2} - R_{NO_3} - R_{SO_4}$):

$$R_{CH_4} = \frac{\kappa_{O_2}^i}{\kappa_{O_2}^i + [O_2]} \cdot \frac{\kappa_{NO_3}^i}{\kappa_{NO_3}^i + [NO_3]} \cdot \frac{\kappa_{SO_4}^i}{\kappa_{SO_4}^i + [SO_4]}, \quad (11)$$

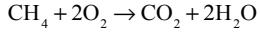
329 where κ_i and κ_i^i terms are as described above (**Table 1**). We disable nitrate (NO₃) as a tracer in the
 330 simulations presented here, such that anaerobic remineralization of organic matter is partitioned
 331 entirely between sulfate reduction and methanogenesis (**Fig. 1**). Using our default parameter
 332 values (**Table 1**), aerobic respiration dominates organic matter remineralization at [O₂] values
 333 significantly above 1 μmol kg⁻¹ (**Fig. 1a**) while anaerobic remineralization is dominated by
 334 methanogenesis at [SO₄²⁻] values significantly below 1 mmol kg⁻¹ (**Fig. 1b**). An important outcome
 335 of the revised ‘inhibition’ scheme is that metabolic pathways with differing intrinsic free energy
 336 yields can coexist, which more accurately reflects field observations from a range of natural
 337 settings (Curtis, 2003;Bethke et al., 2008;Kuivila et al., 1989;Jakobsen and Postma, 1999). In
 338 particular, it allows us to roughly capture the impact of oxidant gradients within sinking marine
 339 aggregates (Bianchi et al., 2018), which can facilitate non-trivial anaerobic carbon
 340 remineralization within sinking particles even in the presence of relatively high [O₂] in the ocean
 341 water column (**Fig. 1c**).

342
 343 While the model tracks the carbon isotope composition of oceanic and atmospheric CH₄ (δ¹³C,
 344 reported in per mil notation relative to the Pee Dee Belemnite, PDB), the only significant isotope
 345 effect we include here is that attendant to acetoclastic methanogenesis. We specify a constant
 346 isotope fractionation between organic carbon and CH₄ during methanogenesis of -35‰ by default
 347 (**Table 2**), which will tend to produce microbial CH₄ with a δ¹³C composition of roughly -60‰
 348 when combined with the default isotope fractionation associated with photosynthetic carbon
 349 fixation in the surface ocean (e.g., Kirtland Turner and Ridgwell, 2016). The model does not
 350 currently include any potential isotope effects associated with aerobic/anaerobic methanotrophy,
 351 air-sea gas exchange of CH₄, or photochemical breakdown of CH₄ in the atmosphere. It does,
 352 however, include a comprehensive ¹³C scheme associated with ocean-atmosphere cycling of CO₂
 353 (Kirtland Turner and Ridgwell, 2016;Ridgwell, 2001).

354

355 3.2. Aerobic methanotrophy

356 Microbial aerobic methanotrophy proceeds according to:



357 This reaction is highly favorable energetically, with a free energy yield under standard conditions
358 of ~850 kJ per mole of methane consumed (**Table 2**). We represent rates of aerobic methanotrophy
359 (R_{AER}) with a mixed kinetic-thermodynamic formulation (Jin & Bethke, 2005; 2007; Regnier et
360 al., 2011), in which CH_4 oxidation kinetics are controlled by substrate availability, thermodynamic
361 energy yield, and temperature:

$$R_{AER} = k_{AER} \cdot F_k^{AER} \cdot F_t^{AER} \cdot F_T \quad (12)$$

362 A rate constant for aerobic methanotrophy (y^{-1}) is defined as k_{AER} , while F_i terms denote kinetic
363 (k) and thermodynamic (t) factors as defined below and a temperature (T) factor as given in Eq.
364 (6) above.

365

366 The kinetic factor (F_k) for aerobic methanotrophy is controlled by substrate availability according
367 to:

$$F_k^{AER} = [\text{CH}_4] \cdot \frac{[\text{O}_2]}{\kappa_O^{AER} + [\text{O}_2]}, \quad (13)$$

368 where brackets denote concentration and the κ term denotes a half-saturation constant with respect
369 to O_2 . We employ a hybrid parameterization in which kinetics are first-order with respect to CH_4
370 but also scaled by a Michaelis-Menten-type term for O_2 . This formulation is based on the rationale
371 that half-saturation constants for CH_4 are typically similar to (or greater than) the dissolved CH_4
372 levels attained in anoxic water column environments (Regnier et al., 2011) but is also meant to
373 allow for rapid CH_4 consumption under ‘bloom’ conditions with an appropriately scaled rate
374 constant (see below).

375

376 The effect of thermodynamic energy yield on aerobic methanotrophy is given by:

$$F_t^{AER} = 1 - \exp\left[\frac{\Delta G_{r,AER} + \Delta G_{BQ,AER}}{\chi RT}\right], \quad (14)$$

377 where ΔG_r denotes the Gibbs free energy of reaction under *in-situ* conditions, ΔG_{BQ} represents the
378 minimum energy required to sustain ATP synthesis (Hoehler et al., 2001; Hoehler, 2004; Jin and

379 Bethke, 2007), χ is the stoichiometric number of the reaction (e.g., the number of times the rate-
 380 determining step occurs in the overall process), and R and T represent the gas constant and absolute
 381 *in-situ* temperature, respectively. The available free energy is estimated according to:

$$\Delta G_{r,AER} = \Delta G_{r,AER}^0 + RT \cdot \ln \frac{\gamma_{CO_2}[CO_2]}{\gamma_{O_2}[O_2] \cdot \gamma_{CH_4}[CH_4]}, \quad (15)$$

382 where, in addition to the terms defined above, ΔG_{r}^0 represents the Gibbs free energy of the reaction
 383 under standard conditions, and γ_i values represent activity coefficients. Note that we assume an
 384 H₂O activity of unity.

385

386 3.3. Anaerobic oxidation of methane (AOM)

387 The oxidation of methane can also be coupled to electron acceptors other than O₂, including nitrate
 388 (NO₃⁻), sulfate (SO₄²⁻), and oxide phases of iron (Fe) and manganese (Mn) (Reeburgh,
 389 1976;Martens and Berner, 1977;Hoehler et al., 1994;Hinrichs et al., 1999;Orphan et al.,
 390 2001;Sivan et al., 2011;Haroon et al., 2013;Egger et al., 2015). Because it is by far the most
 391 abundant of these oxidants on the modern Earth, and has likely been the most abundant throughout
 392 Earth's history, we focus on anaerobic oxidation of methane (AOM) at the expense of SO₄²⁻:



393 This process is currently thought to be performed most often through a syntrophic association
 394 between Archaea and sulfate reducing bacteria (Boetius et al., 2000), though the mechanics
 395 controlling the exchange of reducing equivalents within the syntrophy remain to be fully elucidated
 396 (Milucka et al., 2012;McGlynn et al., 2015). In any case, consumption of CH₄ at the sulfate-
 397 methane transition zone (SMTZ) represents an extremely large sink flux of CH₄ in modern marine
 398 sediments (Regnier et al., 2011;Egger et al., 2018).

399

400 Anaerobic methanotrophy is much less energetically favorable under standard conditions, with a
 401 free energy yield of ~30 kJ per mole of CH₄ (**Table 2**). As a result, the influence of
 402 thermodynamics on rates of AOM is potentially much stronger than it will tend to be in the case
 403 of aerobic methanotrophy. As above, rates of AOM are controlled by the combined influence of
 404 substrate availability, thermodynamic drive, and temperature:

$$R_{AOM} = k_{AOM} \cdot F_k^{AOM} \cdot F_t^{AOM} \cdot F_T \quad (16)$$

405 where k_{AOM} is a rate constant for anaerobic methane oxidation (y^{-1}), while F_i terms denote kinetic
 406 (k) and thermodynamic (t) factors as defined below and a temperature (T) factor as given in Eq.
 407 (6) above.

408

409 The kinetics of anaerobic methane oxidation are specified according to:

$$F_k^{AOM} = [\text{CH}_4] \cdot \frac{[\text{SO}_4^{2-}]}{\kappa_S^{AOM} + [\text{SO}_4^{2-}]} \quad (17)$$

410 where brackets denote concentration and the κ term denotes a half-saturation constant with respect
 411 to SO_4^{2-} . We employ a hybrid parameterization in which kinetics are first-order with respect to
 412 CH_4 but are also scaled by a Michaelis-Menten-type term for SO_4^{2-} for reasons discussed above.

413

414 The effect of thermodynamic energy yield on anaerobic methane oxidation is specified as follows:

$$F_t^{AOM} = 1 - \exp\left[\frac{\Delta G_{r,AOM} + \Delta G_{BQ,AOM}}{\chi RT}\right] \quad (18)$$

415 As above, ΔG_r denotes the Gibbs free energy of reaction under *in-situ* conditions, ΔG_{BQ} is the
 416 minimum energy required to sustain ATP synthesis (the ‘biological quantum’), χ is the
 417 stoichiometric number of the reaction, and R and T represent the gas constant and absolute *in-situ*
 418 temperature, respectively. The available free energy for AOM under *in-situ* conditions is estimated
 419 according to:

$$\Delta G_{r,AOM} = \Delta G_{r,AOM}^0 + RT \cdot \ln \frac{\gamma_{\text{HCO}_3^-} [\text{HCO}_3^-] \cdot \gamma_{\text{HS}^-} [\text{HS}^-]}{\gamma_{\text{SO}_4^{2-}} [\text{SO}_4^{2-}] \cdot \gamma_{\text{CH}_4} [\text{CH}_4]} \quad (19)$$

420 where ΔG_r^0 again represents the Gibbs free energy of the net AOM reaction given above under
 421 standard conditions, and γ_i values represent activity coefficients. Again, we assume an H_2O
 422 activity of unity.

423

424 3.4. Default parameters for aerobic and anaerobic methanotrophy

425 We choose default rate constants according to a dataset of compiled rates of aerobic and anaerobic
 426 methanotrophy in oxygenated and anoxic marine water column environments (see Supplementary
 427 Data), after correction to *in-situ* temperature (**Fig. 2a, b**). Our default values for both rate constants
 428 are on the low end of the observational dataset, but are very roughly tuned to yield steady-state

429 diffusive CH₄ fluxes from the ocean that are consistent with recent observational constraints (**Fig.**
430 **2c**). It is important to note, however, that these values are not extensively tuned and could be
431 adjusted depending on the application. For example, transient CH₄ release experiments could
432 employ rate constants that are scaled upward to reflect transient ('bloom') elevations in microbial
433 community CH₄ consumption as observed in field studies (Kessler et al., 2011; Crespo-Medina et
434 al., 2014). Default values for other kinetic parameters (**Table 2**) are chosen to be broadly consistent
435 with field measurements and pure/mixed culture experiments with aerobic methanotrophs (Bender
436 and Conrad, 1992, 1993; Hanson and Hanson, 1996; Dunfield and Conrad, 2000; van Bodegom et
437 al., 2001), and to remain roughly consistent with previous work for comparative purposes (e.g.,
438 Olson et al., 2016), though the parameters have not been formally tuned and we explore model
439 sensitivity below.

440

441 Thermodynamic energy yields of each reaction under standard conditions are calculated based on
442 the standard molal thermodynamic properties given in Regnier et al. (2011). Stoichiometric
443 numbers are assumed identical for both metabolisms, with default values of 1.0 (Jin and Bethke,
444 2005; Dale et al., 2006). We assume a default biological quantum (ΔG_{BQ}) of 15 kJ mol⁻¹ for both
445 aerobic and anaerobic methanotrophy, though these can be expected to vary somewhat as a
446 function of metabolism and environmental conditions (Schink, 1997; Hoehler, 2004; Dale et al.,
447 2008). These can be varied independently for aerobic and anaerobic methanotrophy in the model,
448 and we explore model sensitivity to this parameter below. Lastly, for simplicity and to minimize
449 computational expense we assume constant activity coefficients for each species throughout all
450 ocean grid cells (**Table 2**). For some applications it may ultimately be important to add a scheme
451 for estimating activity coefficients according to ambient salinity and ion chemistry, for example
452 estimating methane fluxes in planetary scenarios with very different major ion chemistry or much
453 higher/lower salinity than those characteristic of Earth's modern oceans.

454

455 **4. Atmospheric methane cycling**

456 **4.1. Air-sea gas exchange**

457 Ocean-atmosphere fluxes of CH₄ (J_{gas}) are governed by temperature- and salinity-dependent
458 solubility and surface wind speed above a given grid cell:

$$J_{gas} = A \cdot k_{gas} \cdot ([CH_4]_{sat} - [CH_4]_{cell}) \quad (20)$$

459 where A denotes the area available for gas-exchange (e.g., the area of ice-free surface ocean),
 460 $[CH_4]_{cell}$ denotes the ambient dissolved CH_4 concentration in a given surface ocean grid cell,
 461 $[CH_4]_{sat}$ represents the dissolved CH_4 concentration at saturation with a given atmospheric pCH_4 ,
 462 temperature, and salinity, and k_{gas} represents a gas transfer velocity. Solubility is based on a Bunsen
 463 solubility coefficient (β) corrected for ambient temperature (T) and salinity (S) according to:

$$\ln \beta = a_1 + a_2(100/T) + a_3 \ln(T/300) + S[b_1 + b_2(T/100) + b_3(T/100)^2] \quad (21)$$

464 [Note that the Henry's law constant K_0 is related to the Bunsen solubility coefficient by $K_0 =$
 465 $\beta/\rho V^+$, where ρ is density and V^+ is the molar volume of the gas at STP.] Gas transfer velocity
 466 (k_{gas}) is calculated based on the surface windspeed (u) and a Schmidt number (Sc) corrected for
 467 temperature assuming a constant salinity of 35‰:

$$k_{gas} = k \cdot u^2 \cdot [Sc / 660]^{-0.5} \quad (22)$$

468 where k is a dimensionless gas transfer coefficient, u is surface wind speed, and Sc is the
 469 temperature-corrected Schmidt number according to:

$$Sc = c_1 - c_2 T + c_3 T^2 - c_4 T^3 \quad (23)$$

470 All default constants and coefficients for the gas exchange scheme are given in **Table 3**. Overall,
 471 the scheme for air-sea gas exchange of CH_4 follows by default that for other gases accounted for
 472 in BIOGEM, such as O_2 and CO_2 , as described in (Ridgwell et al., 2007)

473 474 **4.2. Parameterized O_2 - O_3 - CH_4 photochemistry**

475 Once degassed to the atmosphere, CH_4 becomes involved in a complex series of photochemical
 476 reactions initiated by hydroxyl radical (OH) attack on CH_4 (Kasting et al., 1983; Prather,
 477 1996; Pavlov et al., 2000; Schmidt and Shindell, 2003). Following Claire et al. (2006) and Goldblatt
 478 et al. (2006), we parameterize O_2 - O_3 - CH_4 photochemistry according to a bimolecular 'rate law':

$$J_{CH_4} = k_{eff} \cdot M_{O_2} \cdot M_{CH_4} \quad (24)$$

479 where M_i terms represent the atmospheric inventories of O_2 and CH_4 , respectively, and k_{eff} denotes
 480 an effective rate constant ($Tmol^{-1} y^{-1}$) that is itself a complicated function of atmospheric O_2 , CH_4 ,
 481 and CO_2 (Claire et al., 2006). We note that in this parameterization, O_3 abundance is not calculated
 482 explicitly, but rather the photochemical destruction rate of CH_4 in the atmosphere is controlled by

483 the combined atmospheric chemistry implicitly embedded within k_{eff} (Goldblatt et al., 2006; Claire
484 et al., 2006).

Formatted: Font: Italic

Formatted: Font: Italic, Subscript

485
486 At each timestep, the distribution of chemical species (e.g., other than temperature and humidity)
487 in the atmosphere is homogenized (Ridgwell et al., 2007) and k_{eff} is estimated based on the resulting
488 instantaneous mean partial pressures of O₂ and CH₄ according to a bivariate fit to a large suite of
489 1-D atmospheric photochemical models. These photochemical model results (Claire, *personal*
490 *communication*) are derived following Claire et al. (2006). Briefly, values for k_{eff} are computed by
491 a 1-D model of atmospheric photochemistry assuming a range of fixed surface mixing ratios of O₂
492 and CH₄ and a constant atmospheric CO₂ of 10⁻² bar. We then fit a fifth-order polynomial surface
493 to these k_{eff} values as a function of atmospheric pO_2 and pCH_4 (**Fig. 3**).

494
495 Our default parameterization of O₂-O₃-CH₄ chemistry (C06) is fit over a pO_2 range of 10⁻¹⁴ to 10⁻¹
496 bar, a pCH_4 range of 10⁻⁶ to 2 x 10⁻³ bar, and a constant high background pCO_2 of 10⁻² bar (Claire
497 et al., 2006). We thus truncate the atmospheric lifetime of CH₄ at a lower bound of 7.6 years in
498 our default parametrization, and provide an alternative parameterization of photochemical CH₄
499 destruction at roughly modern pO_2 and pCO_2 (SS03) derived from the results of Schmidt and
500 Shindell (2003) for use in more geologically recent, high-O₂ atmospheres (Reinhard et al., 2017)
501 (**Fig. 4a**). Although this parameterized photochemistry scheme should represent an improvement
502 in accuracy relative to that implemented in Olson et al. (2016) (see Daines and Lenton, 2016), it
503 is important to point out that a range of factors that might be expected to impact the photochemical
504 destruction rates of CH₄ in the atmosphere, including atmospheric pCO_2 , the atmospheric profile
505 of H₂O, and spectral energy distribution (SED), have not yet been rigorously assessed. Ongoing
506 model developments in ATCHEM are aimed at implementing a more flexible and inclusive
507 photochemical parameterization that will allow for robust use across a wider range of atmospheric
508 compositions and photochemical environments.

509
510 As a basic test of our photochemical parameterization, we impose a terrestrial (wetland) flux of
511 CH₄ to the atmosphere (balanced by stoichiometric consumption of CO₂ and release of O₂), and
512 allow the oceanic and atmospheric CH₄ cycle to spin up for 20 kyr. We then compare steady-state
513 atmospheric pCH_4 as a function of terrestrial CH₄ flux to estimates for the last glacial,

514 preindustrial, and modern periods. Our default parameterization is relatively simple and spans a
515 very wide range in atmospheric O₂ and CH₄ inventories. Nevertheless, both the default scheme
516 and the alternative parameterization for recent geologic history (and analogous planetary
517 environments) with high-*p*O₂/low-*p*CO₂ atmospheres accurately reproduce atmospheric *p*CH₄
518 values given estimated glacial, preindustrial, and modern terrestrial CH₄ fluxes (**Fig. 4C**), and both
519 display the predicted saturation of CH₄ sinks at elevated atmospheric CH₄ observed in more
520 complex photochemical models. We note, however, the alternative parameterization tends to yield
521 slightly higher atmospheric *p*CH₄ at surface fluxes greater than ~50 Tmol y⁻¹ (**Fig. 4C**). (In the
522 remainder of the manuscript, we employ the default (C06) parameterization for atmospheric O₂-
523 O₃-CH₄ chemistry and do not discuss the simple high-*p*O₂/low-*p*CO₂ alternative further.)
524

525 **5. Example applications of the new capabilities in the cGENIE model**

526 **5.1. High-*p*O₂ ('modern') steady state**

527 We explore a roughly modern steady state with appropriate continental geography and simulated
528 overturning circulation (as in Cao et al., 2009) and initialize the atmosphere with *p*O₂, *p*CO₂, and
529 *p*CH₄ of [v/v] 20.95%, 278 ppm, and 700 ppb, respectively, and with globally uniform oceanic
530 concentrations of SO₄²⁻ (28 mmol kg⁻¹) and CH₄ (1 nmol kg⁻¹). We fix globally averaged solar
531 insolation at the modern value (1368 W m⁻²) with seasonally variable forcing as a function of
532 latitude, and set radiative forcing for CO₂ and CH₄ equivalent to preindustrial values in order to
533 isolate the effects of biogeochemistry on steady state tracer distributions. The model is then spun
534 up for 20 kyr with atmospheric *p*O₂ and *p*CO₂ (and δ¹³C of atmospheric CO₂) restored to
535 preindustrial values at every timestep, and with an imposed wetland flux of CH₄ to the atmosphere
536 of 20 Tmol yr⁻¹ that has a δ¹³C value of -60‰. Atmospheric *p*CH₄ and all oceanic tracers are
537 allowed to evolve freely.
538

539 Surface, benthic, and ocean interior distributions of dissolved oxygen (O₂), sulfate (SO₄²⁻), and
540 methane (CH₄) are shown in **Fig. 5** for our roughly modern simulation. Dissolved O₂ ([O₂])
541 approaches air saturation throughout the surface ocean, with a distribution that is largely uniform
542 zonally and with concentrations that increase with latitude as a result of increased solubility at
543 lower temperature near the poles (**Fig. 5a**). Benthic [O₂] shows patterns similar to those expected
544 for the modern Earth, with relatively high values in the well-ventilated deep North Atlantic, low

545 values in the deep North Pacific and Indian oceans, and a gradient between roughly air saturation
546 near regions of deep convection in the high-latitude Atlantic and much lower values in the tropical
547 and northern Pacific (**Fig. 5d**). Distributions of $[O_2]$ in the ocean interior are similar to those of the
548 modern Earth (**Fig. 5g**) with oxygen minimum zones (OMZs) at intermediate depths underlying
549 highly productive surface waters, particularly in association with coastal upwelling at low
550 latitudes.

551

552 Concentrations of dissolved SO_4^{2-} ($[SO_4^{2-}]$) are largely invariant throughout the ocean, consistent
553 with its expected conservative behavior in the modern ocean as one of the most abundant negative
554 ions in seawater (**Fig. 5**). Slightly higher concentrations in both surface and benthic fields are seen
555 in association with outflow from the Mediterranean, and are driven by evaporative concentration
556 (**Fig. 5b**). Benthic $[SO_4^{2-}]$ distributions show some similarity to those of $[O_2]$ (**Fig. 5e**), though
557 again the differences are very small relative to the overall prescribed initial tracer inventory of 28
558 $mmol\ kg^{-1}$ and disappear almost entirely when salinity-normalized (not shown). In the ocean
559 interior, $[SO_4^{2-}]$ is largely spatially invariant with a value of approximately $28\ mmol\ kg^{-1}$ (**Fig. 5h**).

560

561 Dissolved CH_4 concentrations ($[CH_4]$) in the surface and shallow subsurface ocean are much more
562 variable, but typically on the order of $\sim 1\text{-}2\ mmol\ kg^{-1}$ with slightly elevated concentrations just
563 below the surface, both of which are consistent with observations from the modern ocean
564 (Reeburgh, 2007;Scranton and Brewer, 1978). The benthic $[CH_4]$ distribution shows locally
565 elevated values up to $\sim 300\text{-}400\ mmol\ kg^{-1}$ in shallow regions of the tropical and northern Pacific
566 and the Indian oceans (**Fig. 5f**), which is also broadly consistent with observations from shallow
567 marine environments with active benthic CH_4 cycling (Jayakumar et al., 2001). Within the ocean
568 interior, dissolved CH_4 can accumulate in the water column in excess of $\sim 100\ mmol\ kg^{-1}$ in
569 association with relatively low- O_2 conditions at intermediate depths, with zonally averaged values
570 as high as $\sim 70\ mmol\ kg^{-1}$ but more typically in the range of $\sim 20\text{-}40\ mmol\ kg^{-1}$ (**Fig. 5i**). These
571 concentrations are comparable to those observed locally in low- O_2 regions of the modern ocean
572 (Sansone et al., 2001;Chronopoulou et al., 2017;Thamdrup et al., 2019).

573

574 The major metabolic fluxes within the ocean's microbial CH_4 cycle for our 'modern' configuration
575 are shown in Figure 6. Methanogenesis is focused in regions characterized by relatively low $[O_2]$

Deleted: Figure 6 shows the

Formatted: Font: Not Bold

Formatted: Font: Not Bold

Formatted: Font: Bold

577 and is particularly vigorous in the Eastern Tropical Pacific, the North Pacific, and the Indian
578 Ocean (**Fig. 6a**). The highest zonally averaged rates of methanogenesis are observed in northern
579 tropical and subtropical latitudes, and are focused at a depth of ~ 1 km (**Fig. 6d**). Rates of microbial
580 CH_4 consumption are generally spatially coupled to rates of methanogenesis, both in a column-
581 integrated sense (**Fig. 6b, c**) and in the zonal average (**Fig. 6e, f**). This is particularly true for AOM,
582 rates of which are highest within the core of elevated methanogenesis rates observed in the
583 northern subtropics. Zonally averaged AOM rates of ~ 10 - $15 \text{ nmol kg}^{-1} \text{ d}^{-1}$ compare well with field
584 measurements of AOM within oceanic OMZs (Thamdrup et al., 2019). In general, the bulk of CH_4
585 produced via microbial methanogenesis is consumed via AOM, either near the seafloor or within
586 the ocean interior.

587

588 **5.2. Low- $p\text{O}_2$ ('ancient') steady state**

589 Next, we explore a low- $p\text{O}_2$ steady state, similar to the Proterozoic Earth (Reinhard et al., 2017)
590 but played out in a modern continental configuration and overturning circulation, by initializing
591 the atmosphere with $p\text{O}_2$, $p\text{CO}_2$, and $p\text{CH}_4$ of $[\text{v/v}] 2.1 \times 10^{-4} \text{ atm}$ (equivalent to a value 10^{-3} times
592 the present atmospheric level, PAL), 278 ppm, and 500 ppm, respectively, and globally uniform
593 oceanic concentrations of SO_4^{2-} ($280 \mu\text{mol kg}^{-1}$) and CH_4 ($50 \mu\text{mol kg}^{-1}$). We again fix globally
594 averaged solar insolation at the modern value (1368 W m^{-2}) with seasonally variable forcing as a
595 function of latitude, and set radiative forcing for CO_2 and CH_4 equivalent to the modern
596 preindustrial state in order to isolate the effects of biogeochemistry on steady state tracer
597 distributions. The model is then spun up for 20 kyr with atmospheric $p\text{O}_2$ and $p\text{CO}_2$ (and $\delta^{13}\text{C}$ of
598 atmospheric CO_2) restored to the initial values specified above at every timestep, with an imposed
599 'geologic' flux of CH_4 to the atmosphere of 3 Tmol yr^{-1} at a $\delta^{13}\text{C}$ value of -60‰ . Atmospheric
600 $p\text{CH}_4$ and all oceanic tracers are allowed to evolve freely.

601

602 Surface, benthic, and ocean interior distributions of $[\text{O}_2]$, $[\text{SO}_4^{2-}]$, and $[\text{CH}_4]$, are shown in **Fig. 7**
603 for our low- $p\text{O}_2$ simulation. Dissolved O_2 concentrations are now extremely heterogeneous
604 throughout the surface ocean, ranging over an order of magnitude from less than $1 \mu\text{mol kg}^{-1}$ to
605 over $10 \mu\text{mol kg}^{-1}$, with concentrations that are regionally well in excess of air saturation at the
606 prescribed $p\text{O}_2$ of $2.1 \times 10^{-4} \text{ atm}$ (**Fig. 7a**). Previous studies have shown that these features are not
607 unexpected at very low atmospheric $p\text{O}_2$ (Olson et al., 2013; Reinhard et al., 2016). We note,

608 however, that the distribution and maximum $[O_2]$ in our low- pO_2 simulation are both somewhat
609 different from those presented in Olson et al. (2013) and Reinhard et al. (2016). We attribute this
610 primarily to the different parameterizations of primary production in the surface ocean. In the
611 biogeochemical configuration of cGENIE we adopt here, we allow rates of photosynthesis to scale
612 more directly with available PO_4^{3-} than is the case in these previous studies (Eq. 3), which allows
613 for higher rates of oxygen production in regions of deep mixing and relatively intense organic
614 matter recycling below the photic zone (**Fig. 7a**). In any case, as in previous examinations of
615 surface $[O_2]$ dynamics at low atmospheric pO_2 (Olson et al., 2013; Reinhard et al., 2016), our
616 regional $[O_2]$ patterns still generally track the localized balance between photosynthetic O_2 release
617 and consumption through respiration and reaction with inorganic reductants, rather than
618 temperature-dependent solubility patterns (**Fig. 5a**). Within the ocean interior, O_2 is consumed
619 within the upper few hundred meters and is completely absent in benthic settings (**Fig. 7d, g**).

620

621 In our low- pO_2 simulations we initialize the ocean with a globally uniform $[SO_4^{2-}]$ of $280 \mu\text{mol}$
622 kg^{-1} , under the premise that marine SO_4^{2-} inventory should scale positively with atmospheric pO_2 .
623 With this much lower initial SO_4^{2-} inventory (i.e., 10^2 times less than the modern ocean), steady
624 state $[SO_4^{2-}]$ distributions are significantly more heterogeneous than in the modern, high- pO_2 case
625 (**Fig. 7**). Ocean $[SO_4^{2-}]$ is approximately homogeneous spatially in surface waters, even with a
626 significantly reduced seawater inventory (**Fig. 7a**), but is strongly variable within the ocean interior
627 (**Fig. 7e, h**). Indeed, in our low- pO_2 simulations SO_4^{2-} serves as the principal oxidant for organic
628 matter remineralization in the ocean interior, with the result that its distribution effectively mirrors
629 that of $[O_2]$ in the modern case in both spatial texture and overall magnitude (compare **Fig. 7e, h**
630 with **Fig. 5d, g**). Dissolved SO_4^{2-} in this simulation never drops to zero, a consequence of our initial
631 $280 \mu\text{mol kg}^{-1}$ concentration of SO_4^{2-} representing the oxidative potential of $560 \mu\text{mol kg}^{-1}$ of O_2 ,
632 some 3 times higher than the mean $[O_2]$ value in the modern ocean interior ($\sim 170 \mu\text{mol kg}^{-1}$).

633

634 Dissolved CH_4 concentrations in the surface and shallow subsurface ocean are variable but much
635 higher than in our modern simulations, typically on the order of $\sim 1\text{-}2 \mu\text{mol kg}^{-1}$ (**Fig. 7c**). The
636 benthic $[CH_4]$ distribution shows concentrations up to $\sim 8 \mu\text{mol kg}^{-1}$, with concentrations in excess
637 of $1 \mu\text{mol kg}^{-1}$ pervasively distributed across the seafloor. In general, the benthic $[CH_4]$ distribution
638 inversely mirrors that of $[SO_4^{2-}]$ (**Fig. 7f**), which results from the fact that in the low- pO_2 case

639 SO_4^{2-} again serves as the principal oxidant of methane. Concentrations of CH_4 in the ocean interior
640 can approach $\sim 10 \mu\text{mol kg}^{-1}$, but in the zonal average are typically less than $5 \mu\text{mol kg}^{-1}$ (**Fig. 7i**).
641 Overall, the oceanic CH_4 inventory increases dramatically in the low- $p\text{O}_2$ case relative to the
642 modern simulation, from $\sim 4.5 \text{ Tmol CH}_4$ to $\sim 1900 \text{ Tmol CH}_4$.

643

644 ~~The major metabolic fluxes within the ocean's microbial CH_4 cycle for our 'ancient' configuration~~
645 ~~are shown in Figure 8.~~ Column-integrated rates of microbial methanogenesis are greater than in
646 the high- $p\text{O}_2$ case by up to a factor of $\sim 10^2$ (**Fig. 8a**), with methanogenesis also showing a much
647 broader areal distribution. Within the ocean interior, rates of methanogenesis are most elevated in
648 the upper $\sim 1 \text{ km}$ (**Fig. 8d**) as a consequence of elevated rates of organic carbon remineralization
649 combined with a virtual absence of dissolved O_2 beneath the upper $\sim 200 \text{ m}$. Rates of aerobic
650 methanotrophy, which is effectively absent in the ocean interior (**Fig. 8e**), are elevated relative to
651 those observed the high- $p\text{O}_2$ simulation by less than an order of magnitude and are concentrated
652 in the tropical surface ocean near the equatorial divergence (**Fig. 8b**). In contrast, AOM is strongly
653 coupled spatially to microbial methanogenesis, with rates that are often well over $\sim 10^2$ times higher
654 than those observed in the high- $p\text{O}_2$ case (**Fig. 8c, f**). Once again, AOM dominates the
655 consumption of CH_4 produced in the ocean interior and ~~is extremely effective at reducing CH_4~~
656 fluxes to the atmosphere. Despite a significant increase in overall oceanic CH_4 burden relative to
657 our high- $p\text{O}_2$ simulation (see above and **Fig. 7i**), atmospheric $p\text{CH}_4$ increases only modestly from
658 $\sim 0.8 \text{ ppm}$ to 6 ppm [v/v] , equivalent to an additional radiative forcing of only $\sim 2 \text{ W m}^{-2}$, due to
659 efficient microbial consumption in the upper ocean.

660

661 5.3. Atmospheric carbon injection

662 To illustrate the capabilities of the model in exploring the time-dependent (perturbation) behavior
663 of the CH_4 cycle, we perform a simple carbon injection experiment in which $3,000 \text{ PgC}$ are injected
664 directly into the atmosphere either as CH_4 or as CO_2 , starting from our modern steady state. The
665 injection is spread over 1,000 years, with an instantaneous initiation and termination of carbon
666 input to the atmosphere. ~~This is meant only to illustrate the time-dependent behavior of the model~~
667 ~~in the face of an idealized carbon cycle perturbation, rather than to evaluate any particular scenario~~
668 ~~for explaining previous climate transients in Earth's history. However, the magnitude and duration~~
669 of this carbon injection, corresponding to 3 PgC y^{-1} , is meant to roughly mimic the upper end of

Deleted: Figure 8 shows the

Formatted: Font: Not Bold

Deleted: acts as an extremely effective throttle on

Deleted: T

673 estimates for the Paleocene-Eocene Thermal Maximum, a transient global warming event at ~56
674 Ma hypothesized to have been driven by emissions of CO₂ and/or CH₄ (Kirtland Turner, 2018).
675 This flux is much lower than the current anthropogenic carbon input of ~10 PgC y⁻¹ (Ciais et al.,
676 2013). For simplicity, and because we focus on only the first 3,000 years following carbon
677 injection, we treat the ocean-atmosphere system as closed, with the result that all injected carbon
678 ultimately accumulates within the ocean and atmosphere rather than being removed through
679 carbonate compensation and silicate weathering.

680

681 Following a carbon release to the atmosphere in the form of CH₄, there is an immediate and
682 significant increase in atmospheric *p*CH₄ to values greater than 10 ppmv, followed by a gradual
683 increase to a maximum of ~12 ppmv throughout the duration of the CH₄ input (**Fig. 9a**). Much of
684 this methane is exchanged with the surface ocean and consumed by aerobic methanotrophy, while
685 some is photochemically oxidized directly in the atmosphere, both of which lead to a significant
686 but delayed increase in atmospheric *p*CO₂ (**Fig. 9b**). This increase in atmospheric *p*CH₄ and *p*CO₂
687 leads to an increase in global average surface air temperature (SAT) of ~7°C (**Fig. 9d**), an increase
688 in mean ocean temperature (MOT) of ~2°C (**Fig. 9e**), along with significant acidification of the
689 surface ocean (**Fig. 9c**).

690

691 The increase in atmospheric *p*CO₂ and drop in ocean pH are nearly identical if we instead inject
692 the carbon as CO₂ rather than CH₄. (**Fig. 9b, c**). However, when carbon is injected as CH₄, there
693 is an additional transient increase in global surface air temperature of ~2°C and roughly 0.5°C of
694 additional whole ocean warming for the same carbon input and duration (**Fig. 9f**). This results
695 from the fact that mole-for-mole, CH₄ is a much more powerful greenhouse gas than is CO₂, and
696 oxidation of CH₄ to CO₂ is not instantaneous during the carbon release interval. Combined, these
697 factors result in a disequilibrium situation in which a proportion of carbon released to the
698 atmosphere remains in the form of CH₄ rather than CO₂, providing an enhancement of warming,
699 especially during the duration of carbon input. This warming enhancement should be considered
700 in past events during which CH₄ release is suspected as a key driver of warming. For instance,
701 additional warming due to CH₄ forcing may help explain the apparent discrepancy between the
702 amount of warming reconstructed by proxy records and proposed carbon forcing during the PETM
703 (Zeebe et al., 2009)

704

705 **5.4. Atmospheric $p\text{CH}_4$ on the early Earth**

706 Using our low- $p\text{O}_2$ steady state as a benchmark case (**Section 5.2**), we briefly explore the
707 sensitivity of atmospheric $p\text{CH}_4$ to a subset of model variables. All model ensembles are initially
708 configured with globally homogeneous marine SO_4^{2-} and CH_4 inventories and a background
709 geologic CH_4 flux of 3 Tmol y^{-1} , and are spun up for 20 kyr with a fixed $p\text{O}_2$ and $p\text{CO}_2$. We report
710 atmospheric $p\text{CH}_4$ from the final model year. Our purpose here is not to be exhaustive or to
711 elucidate any particular period of Earth history, but to demonstrate some of the major factors
712 controlling the atmospheric abundance of CH_4 on a low-oxygen Earth-like planet. We present
713 results from individual sensitivity ensembles from our benchmark low- $p\text{O}_2$ case over the following
714 parameter ranges: (1) atmospheric $p\text{O}_2$ between 10^{-4} to 10^{-1} times the present atmospheric level
715 (PAL), equivalent to roughly 2×10^{-5} and 2×10^{-2} atm, respectively; (2) initial marine SO_4^{2-}
716 inventories corresponding to globally uniform seawater concentrations between 0 and $1,000 \mu\text{mol}$
717 kg^{-1} ; and (3) biological energy quanta (BEQ) for anaerobic methane oxidation between 5 and 30
718 kJ mol^{-1} .

719

720 Results for our low- $p\text{O}_2$ sensitivity ensembles are shown in **Figure 10**. We find a similar sensitivity
721 of atmospheric $p\text{CH}_4$ to atmospheric $p\text{O}_2$ to that observed by (Olson et al., 2016). In particular,
722 atmospheric CH_4 abundance initially increases as atmospheric $p\text{O}_2$ drops below modern values to
723 roughly 2-3% PAL, after which decreasing $p\text{O}_2$ causes $p\text{CH}_4$ to drop. This behavior is well-known
724 from previous 1-D photochemical model analysis, and arises principally from increasing
725 production of OH via water vapor photolysis as shielding of H_2O by ozone (O_3) decreases at low
726 atmospheric $p\text{O}_2$ (Pavlov et al., 2003; Claire et al., 2006; Goldblatt et al., 2006). However, peak
727 atmospheric $p\text{CH}_4$ is significantly reduced in our models relative to those of Olson et al. (2016).
728 For example, at an ‘optimal’ atmospheric $p\text{O}_2$ of $\sim 2.5\%$ PAL Olson et al. (2016) predict a steady
729 state atmospheric $p\text{CH}_4$ of ~ 35 ppmv, while we predict a value of ~ 10 ppmv (**Fig. 10a**). This
730 difference can be attributed to our updated O_2 - O_3 - CH_4 photochemistry parameterization together
731 with a significant upward revision in the rate constant for aerobic methanotrophy. Nevertheless,
732 our results strongly reinforce the arguments presented in Olson et al. (2016), and taken at face
733 value further marginalize the role of CH_4 as a significant climate regulator at steady state during
734 most of the Proterozoic Eon (between ~ 2.5 and 0.5 Ga).

735

736 Atmospheric CH₄ abundance is also strongly sensitive to the marine SO₄²⁻ inventory (**Fig. 10b**).
737 The scaling we observe between initial SO₄²⁻ inventory and steady state atmospheric *p*CH₄ is very
738 similar to that reported by Olson et al. (2016), with a sharp drop in the marine CH₄ inventory and
739 atmospheric CH₄ abundance as marine SO₄²⁻ drops below ~100 μmol kg⁻¹ (**Fig. 10b**). The
740 implication is that for most of Earth history anaerobic oxidation of CH₄ in the ocean interior has
741 served as an important inhibitor of CH₄ fluxes from the ocean biosphere. However, during much
742 of the Archean Eon (between 4.0 and 2.5 Ga), sulfur isotope analysis indicates that marine SO₄²⁻
743 concentrations may instead have been on the order of ~1-10 μmol kg⁻¹ (Crowe et al., 2014), while
744 atmospheric *p*O₂ would also have been much lower than the values examined here (Pavlov &
745 Kasting, 2002). The impact of the ocean biosphere and redox chemistry on atmospheric *p*CH₄ and
746 Earth's climate system may thus have been much more important prior to ~2.5 billion years ago.

747

748 Atmospheric CH₄ is significantly impacted by the value chosen for the biological energy quantum
749 (BEQ). With all other parameters held constant, we observe an increase in steady state atmospheric
750 *p*CH₄ from ~7 ppmv to ~25 ppmv when increasing the BEQ value from 20 to 30 kJ mol⁻¹ (**Fig.**
751 **10c**). This effect is mediated primarily by the importance of anaerobic methanotrophy when
752 atmospheric *p*O₂ is low and the ocean interior is pervasively reducing. The standard free energy of
753 AOM is of the same order of magnitude as the BEQ (see above), which elevates the importance of
754 thermodynamic drive in controlling global rates of AOM. We would expect this effect to be much
755 less important when aerobic methanotrophy is the predominant CH₄ consuming process within the
756 ocean biosphere, as the standard free energy of this metabolism is over an order of magnitude
757 greater than typical BEQ values for microbial metabolism (e.g., Hoehler, 2004). In any case, our
758 results suggest that the role of thermodynamics should be borne in mind in scenarios for which
759 AOM is an important process in the CH₄ cycle and seawater [SO₄²⁻] is relatively low.

760

761 **6. Discussion and Conclusions**

762 The global biogeochemical cycling of CH₄ is central to the climate and redox state of planetary
763 surface environments, and responds to the internal dynamics of other major biogeochemical cycles
764 across a very wide range of spatial and temporal scales. There is thus strong impetus for the
765 ongoing development of a spectrum of models designed to explore planetary CH₄ cycling, from

Deleted: Interestingly, a

767 simple box models to more computationally expensive 3-D models with dynamic and interactive
768 ocean circulation. Our principal goal here is the development of a mechanistically realistic but
769 simple and flexible representation of CH₄ biogeochemical cycling in Earth's ocean-atmosphere
770 system, with the hope that this can be further developed to explore steady state and time-dependent
771 changes to global CH₄ cycle in Earth's past and future and ultimately to constrain CH₄ cycling
772 dynamics on Earth-like planets beyond our solar system.

773

774 To accomplish this, we have refined the organic carbon remineralization scheme in the cGENIE
775 Earth system model to reflect the impact of anaerobic organic matter recycling in sinking
776 aggregates within oxygenated waters, and to include the carbon cycling and isotopic effects of
777 microbial CH₄ production. We have also incorporated revised schemes for microbial CH₄
778 consumption that include both kinetic and thermodynamic constraints, and have updated the
779 parameterized atmospheric O₂-O₃-CH₄ photochemistry to improve accuracy and for use across a
780 wider range of atmospheric *p*O₂ values than that explored in previous work. Simulations of roughly
781 modern (high-O₂) and Proterozoic (low-O₂) Earth system states demonstrate that the model
782 effectively reproduces the first-order features of the modern ocean-atmosphere CH₄ cycle, and can
783 be effectively implemented across a wide range of atmospheric O₂ partial pressures and marine
784 SO₄²⁻ concentrations. In addition, our results strongly reinforce the conclusions of Olson et al.
785 (2016) for the Proterozoic Earth system, while going beyond this to posit that the thermodynamics
786 of anaerobic CH₄ consumption may have been important in regulating atmospheric CH₄ abundance
787 during Archean time. Finally, our simulation of PETM-like carbon injection demonstrates the
788 importance of explicitly considering CH₄ radiative forcing during transient warming events in
789 Earth history.

790

791 We suggest that ongoing and future development work should focus on: (1) more rigorous tuning
792 of organic carbon remineralization and CH₄ production/consumption schemes based on data fields
793 from the modern ocean; (2) development and implementation of a more flexible parameterization
794 of atmospheric photochemistry that allows the roles of atmospheric temperature structure, water
795 vapor abundance, and atmospheric *p*CO₂ to be explored; (3) coupling of deep ocean chemistry
796 with a description of marine methane hydrates and associated sedimentary CH₄ cycling; and (4)
797 developing a representation of the production/consumption of CH₄ by terrestrial ecosystems.

798

799 **7. Model code availability**

800 A manual describing code installation, basic model configuration, and an extensive series of
801 tutorials is provided. The Latex source of the manual and PDF file can be obtained by cloning
802 (<https://github.com/derpycode/muffindoc>). The user manual contains instructions for obtaining,
803 installing, and testing the code, as well as running experiments. The version of the code used in
804 this paper is tagged as release v0.9.14, and has a DOI of 10.5281/zenodo.4002934. Configuration
805 files for the specific experiments presented in the paper can be found in: cgenie.muffin/genie-
806 userconfigs/MS/reinhardetal.GMD.2020. Details of the different experiments, plus the command
807 line needed to run each, are given in README.txt.

808

809 **Author contributions:**

810 CTR, SLO, and AR developed new model code. CTR and CP compiled and analyzed empirical
811 data for rates of methanotrophy. CTR performed all model simulations and data analysis. CTR
812 prepared the manuscript with contributions from all co-authors.

813

814 **Acknowledgements:**

815 This research was supported by funds from the NASA Exobiology Program (proposal 18-EXO18-
816 0005). CTR acknowledges support from the NASA Astrobiology Institute (NAI) and the NASA
817 Nexus for Exoplanet System Science (NExSS). SLO acknowledges support from the T.C.
818 Chamberlin Postdoctoral Fellowship in the Department of Geophysical Sciences at the University
819 of Chicago. AR, SKT, and YK were supported in part by an award from the Heising-Simons
820 Foundation. We also thank Mark Claire for providing unpublished photochemical model results.

821

822 **TABLES:**

823

824 **Table 1.** Default parameters for organic matter production and water column remineralization.

parameter	description	default value	units	source
<i>uptake/photosynthesis</i>				
λ	rate constant for DOM degradation	0.5	y ⁻¹	1
ν	fractional partitioning into DOM	0.66	—	1

Deleted: ¶

Deleted: 0
Deleted: 3620846

Deleted: , the Alfred P. Sloan Foundation,

Deleted: ¶

τ_{bio}	nutrient uptake timescale	63	d	2
κ_I	light limitation term	20	W m ⁻²	3
κ_P	half-saturation constant for PO ₄ uptake	2.1 x 10 ⁻⁷	mol kg ⁻¹	1
k_{T0}	pre-exponential temperature constant	0.59	—	[see text]
k_{eT}	exponential temperature constant	15.8	—	[see text]
<i>organic remineralization</i>				
r_1^{POM}	partitioning into labile POM fraction	0.945	—	1
l_1^{POM}	<i>e</i> -folding depth for labile POM fraction	589	m	[see text]
r_2^{POM}	partitioning into refractory POM fraction	0.055	—	4
l_2^{POM}	<i>e</i> -folding depth for recalcitrant POM fraction	10 ⁶	m	[see text]
κ_{O_2}	half-saturation constant for aerobic respiration	1.0 x 10 ⁻⁷	mol kg ⁻¹	[see text]
$\kappa_{O_2}^i$	inhibition constant for aerobic respiration	1.0 x 10 ⁻⁶	mol kg ⁻¹	[see text]
κ_{SO_4}	half-saturation constant for sulfate reduction	5.0 x 10 ⁻⁴	mol kg ⁻¹	4
$\kappa_{SO_4}^i$	Inhibition constant for sulfate reduction	5.0 x 10 ⁻⁴	mol kg ⁻¹	4

839 ¹Ridgwell et al. (2007); ²Meyer et al. (2016); ³Doney et al. (2006); ⁴Olson et al. (2016)

840

841

842

843

844

845

846 **Table 2.** Default kinetic and thermodynamic parameters for oceanic methane cycling. Activity coefficients

847 are estimated for $T = 25^\circ\text{C}$ and $S = 35\text{‰}$.

parameter	description	default value	units	source
<i>kinetic parameters</i>				
k_{AER}	rate constant for aerobic methanotrophy	0.10	y ⁻¹	[see text]
κ_O^{AER}	half-saturation constant for O ₂	2.0 x 10 ⁻⁵	mol kg ⁻¹	[see text]

k_{AOM}	rate constant for AOM	0.01	y^{-1}	[see text]
K_S^{AOM}	AOM half-saturation constant for SO_4^{2-}	5.0×10^{-4}	$mol\ kg^{-1}$	1
<i>thermodynamic parameters</i>				
$\Delta G_{r,AER}^0$	standard free energy yield of aerobic methanotrophy	-858.967	$kJ\ mol^{-1}$	2
$\Delta G_{r,AOM}^0$	standard free energy yield of AOM	-33.242	$kJ\ mol^{-1}$	2
$\Delta G_{BQ,AER}$	minimum free energy for aerobic methanotrophy	-15.0	$kJ\ mol^{-1}$	[see text]
$\Delta G_{BQ,AOM}$	minimum free energy for AOM	-15.0	$kJ\ mol^{-1}$	2-5
γ_{CH_4}	activity coefficient for dissolved CH_4	1.20	—	6-8
γ_{CO_2}	activity coefficient for aqueous CO_2	1.17	—	9
γ_{O_2}	activity coefficient for dissolved O_2	1.14	—	10
$\gamma_{HCO_3^-}$	activity coefficient for dissolved HCO_3^-	0.58	—	11, 12
γ_{HS^-}	activity coefficient for dissolved HS^-	0.75	—	13
$\gamma_{SO_4^{2-}}$	activity coefficient for dissolved SO_4^{2-}	0.10	—	11
R	gas constant	8.2144×10^{-3}	$kJ\ K^{-1}\ mol^{-1}$	
χ	stoichiometric number	1.0	—	14
<i>isotopic parameters</i>				
ϵ_{CH_4}	methanogenesis isotope effect	-35.0	%	[see text]

848 ¹Olson et al. (2016); ²Regnier et al. (2011); ³Schink (1997); ⁴Hoehler et al. (2001); ⁵Hoehler (2004); ⁶Stoessell and
849 Byrne (1982); ⁷Cramer (1984); ⁸Duan et al. (1992); ⁹Johnson (1982); ¹⁰Clegg and Brimblecombe (1990); ¹¹Ulfbo et
850 al. (2015); ¹²Berner (1965); ¹³Helz et al. (2011); ¹⁴Dale et al. (2008)

851 **Table 3.** Default constants and coefficients for CH_4 gas exchange. All default parameter values derived
852 from Wanninkhof (1992). Schmidt number coefficients are for $S = 35\%$.

parameter	description	default value
a_1	Bunsen temperature coefficient 1	-68.8862
a_2	Bunsen temperature coefficient 2	101.4956
a_3	Bunsen temperature coefficient 3	28.7314

b_1	Bunsen salinity coefficient 1	-0.076146
b_2	Bunsen salinity coefficient 2	0.043970
b_3	Bunsen salinity coefficient 3	-0.0068672
c_1	Schmidt temperature coefficient 1	2039.2
c_2	Schmidt temperature coefficient 2	120.31
c_3	Schmidt temperature coefficient 3	3.4209
c_4	Schmidt temperature coefficient 4	0.040437
k	Gas exchange constant	0.31

853
854
855
856
857
858
859
860
861
862
863
864
865
866
867
868
869
870
871

FIGURES CAPTIONS:

872
873
874
875
876
877
878

Figure 1. Fractional organic carbon remineralization by aerobic respiration, sulfate reduction, and methanogenesis in our modified organic matter remineralization scheme. In (a), relative rates of aerobic (O_2) and anaerobic ($SO_4^{2-} + CH_4$) remineralization are plotted as a function of dissolved $[O_2]$. In (b), relative anaerobic remineralization rates are partitioned between sulfate reduction and methanogenesis as a function of dissolved $[SO_4^{2-}]$ (dissolved $[O_2]$ is held

879 constant at 10^{-10} mol kg⁻¹). Shown in (c) are our estimated anaerobic remineralization fractions (grey curve) compared
880 to estimates from a particle biogeochemical model applied to oxygen minimum zones (OMZs) in the Eastern Tropical
881 South Pacific (ETSP) and Mauritanian upwelling (Bianchi et al., 2018).

882

883 **Figure 2.** Compilation of rate constants for aerobic (AER; a) and anaerobic (AOM; b) methane oxidation. Rate
884 constants are corrected for *in situ* temperature using a Q_{10} of 2 (see Supplementary Materials). Vertical red lines show
885 our default values as reported in **Table 2**. Shown in (c) are globally integrated diffusive fluxes of CH₄ from the ocean
886 for a range of rate constants for aerobic methanotrophy, including our default simulation. The bar to the right of (c)
887 shows the median (black bar) and 90% credible interval (grey shading) for estimates of the modern oceanic diffusive
888 flux from (Weber et al., 2019)

889

890 **Figure 3.** Shown in (a) is the bivariate fit to a suite of 1-D atmospheric photochemical runs for the effective rate
891 constant (k_{eff}) parameterizing O₂-O₃-CH₄ photochemistry in ATCHEM. Shown in (b) is a frequency distribution of the
892 residuals on k_{eff} from the underlying photochemical model output.

893

894 **Figure 4.** Comparison of steady-state atmospheric p CH₄ as a function of terrestrial CH₄ flux with modern/recent
895 estimates. Shown in (a) is an exponential fit to the 2-D photochemistry model of Schmidt and Shindell (2003) (SS03),
896 with individual model runs shown as black crosses. Shown in (b) is a plane through the bivariate fit shown in Figure
897 3 (grey curve), compared with the ensemble of 1-D atmospheric photochemical models at $pO_2 = 0.1$ atm (black
898 crosses; see text). Shown in (c) are steady-state atmospheric CH₄ values as a function of imposed terrestrial CH₄ flux
899 in our 'modern' configuration (circles), compared to estimates for the glacial, preindustrial, and modern CH₄ cycles
900 (Kirschke et al., 2013; Bock et al., 2017; Paudel et al., 2016)

901

902 **Figure 5.** Tracer distributions in surface (a-c) and benthic (d-f) grid cells and in the zonally averaged ocean interior
903 (g-i) for O₂ (a, d, g), SO₄²⁻ (b, e, h), and CH₄ (c, f, i) in our 'modern' configuration. Note different concentration units
904 for each tracer.

905

906 **Figure 6.** Major biological fluxes in the marine methane cycle for our 'modern' configuration. Panels show column
907 integrated (a-c) and zonally averaged (d-f) rates of methanogenesis, aerobic methanotrophy, and anaerobic methane
908 oxidation (AOM) in the ocean interior.

909 **Figure 7.** Tracer distributions in surface (a-c) and benthic (d-f) grid cells and in the zonally averaged ocean interior
910 (g-i) for O₂ (a, d, g), SO₄²⁻ (b, e, h), and CH₄ (c, f, i) in our 'ancient' configuration (see text). Note different
911 concentration units for each tracer, and the differing scales relative to Figure 5.

912

913 **Figure 8.** Major biological fluxes in the marine methane cycle for our 'ancient' configuration. Panels show column
914 integrated (a-c) and zonally averaged (d-f) rates of methanogenesis, aerobic methanotrophy, and anaerobic methane
915 oxidation (AOM) in the ocean interior.

916

917 **Figure 9.** Response to a 3,000 PgC release directly to the atmosphere spread over 1,000 years, assuming carbon is
918 injected as either CH₄ or CO₂. Atmospheric *p*CH₄ (a), *p*CO₂ (b), mean surface ocean pH (c), mean surface air
919 temperature (SAT; d), and mean ocean temperature (MOT; e) are shown for a CH₄ injection (grey) and a CO₂ injection
920 (black). Panel (f) shows the difference in SAT and MOT between the CH₄ and CO₂ injection scenarios ($\Delta T_i = T_{\text{CH}_4,i} -$
921 $T_{\text{CO}_2,i}$) through time.

922

923 **Figure 10.** Sensitivity ensembles of our ‘ancient’ configuration compared to the results of Olson et al. (2016). Steady-
924 state atmospheric *p*CH₄ values as a function of assumed atmospheric *p*O₂ (a) and initial marine SO₄²⁻ inventory (b)
925 are shown for our ‘ancient’ configuration (filled circles; see text) and from Olson et al. (black crosses). Shown below
926 are additional ensembles showing the impact of varying the minimum free energy yield required for microbial methane
927 oxidation (BEQ; c) on atmospheric *p*CH₄. All simulations were spun up from cold for 20 kyr, with the results shown
928 from the last model year.

929

930

931

932

933

934

935

936

937

938

939

940

941

942

943

944

945

946

947

REFERENCES:

948 Archer, D., and Buffett, B.: Time-dependent response of the global ocean clathrate reservoir to
949 climatic and anthropogenic forcing, *Geochemistry Geophysics Geosystems*, 6,
950 10.1029/2004GC000854, 2005.

Formatted: Justified, Indent: Left: 0", Hanging: 0.25"

- ϕ51 Archer, D., Buffett, B., and Brovkin, V.: Ocean methane hydrates as a slow tipping point in the
 952 global carbon cycle, *Proceedings of the National Academy of Sciences, USA*, 106, 20596-
 953 20601, 2009.
- ϕ54 Bartdorff, O., Wallmann, K., Latif, M., and Semenov, V.: Phanerozoic evolution of atmospheric
 955 methane, *Global Biogeochemical Cycles*, 22, 10.1029/2007GB002985, 2008.
- ϕ56 Beerling, D., Berner, R. A., Mackenzie, F. T., Harfoot, M. B., and Pyle, J. A.: Methane and the
 957 CH₄-related greenhouse effect over the past 400 million years, *American Journal of Science*,
 958 309, 97-113, 2009.
- ϕ59 Bender, M., and Conrad, R.: Kinetics of CH₄ oxidation in oxic soils exposed to ambient air or
 960 high CH₄ mixing ratios, *Fems Microbiol Lett*, 101, 261-270, 1992.
- ϕ61 Bender, M., and Conrad, R.: Kinetics of methane oxidation in oxic soils, *Chemosphere*, 26, 687-
 962 696, 1993.
- ϕ63 Berner, R. A.: Activity Coefficients of Bicarbonate Carbonate and Calcium Ions in Sea Water,
 964 *Geochimica Et Cosmochimica Acta*, 29, 947-&, 1965.
- ϕ65 Bethke, C. M., Ding, D., Jin, Q., and Sanford, R. A.: Origin of microbiological zoning in
 966 groundwater flows, *Geology*, 36, 739-742, 2008.
- ϕ67 Bianchi, D., Weber, T. S., Kiko, R., and Deutsch, C.: Global niche of marine anaerobic
 968 metabolisms expanded by particle microenvironments, *Nat Geosci*, 11, 263-268, 2018.
- ϕ69 Bjerrum, C. J., and Canfield, D. E.: Towards a quantitative understanding of the late
 970 Neoproterozoic carbon cycle, *Proceedings of the National Academy of Sciences, USA*, 108,
 971 5542-5547, 2011.
- ϕ72 Bock, M., Schmitt, J., Beck, J., Seth, B., Chappellaz, J., and Fischer, H.: Glacial/interglacial
 973 wetland, biomass burning, and geologic methane emissions constrained by dual stable isotopic
 974 CH₄ ice core records, *Proceedings of the National Academy of Sciences, USA*, 114, E5778-
 975 E5786, 2017.
- ϕ76 Boetius, A., Ravensschlag, K., Schubert, C. J., Rickert, D., Widdel, F., Gieseke, A., Amann, R.,
 977 Jørgensen, B. B., Witte, U., and Pfannkuche, O.: A marine microbial consortium apparently
 978 mediating anaerobic oxidation of methane, *Nature*, 407, 623-626, 2000.
- ϕ79 Boudreau, B. P.: *Diagenetic Models and Their Implementation*, Springer, 1996a.
- ϕ80 Boudreau, B. P.: A method-of-lines code for carbon and nutrient diagenesis in aquatic sediments,
 981 *Computers & Geosciences*, 22, 479-496, 1996b.
- ϕ82 Cao, L., Eby, M., Ridgwell, A., Caldeira, K., Archer, D., Ishida, A., Joos, F., Matsumoto, K.,
 983 Mikolajewicz, U., Mouchet, A., Orr, J. C., Plattner, G.-K., Schlitzer, R., Tokos, K., Totterdell,
 984 I., Tschumi, T., Yamanaka, Y., and Yool, A.: The role of ocean transport in the uptake of
 985 anthropogenic CO₂, *Biogeosciences*, 6, 375-390, 2009.

- φ86 Catling, D. C., Claire, M. W., and Zahnle, K. J.: Anaerobic methanotrophy and the rise of
 987 atmospheric oxygen, *Philosophical Transactions of the Royal Society A*, 365, 1867-1888,
 988 2007.
- φ89 Chapelle, F. H., McMahon, P. B., Dubrovsky, N. M., Fujii, R. F., Oaksford, E. T., and Vroblesky,
 990 D. A.: Deducing the distribution of terminal electron-accepting processes in hydrologically
 991 diverse groundwater systems, *Water Resources Research*, 31, 359-371, 1995.
- φ92 Chronopoulou, P.-M., Shelley, F., Pritchard, W. J., Maanoja, S., and Trimmer, M.: Origin and fate
 993 of methane in the Eastern Tropical North Pacific oxygen minimum zone, *The ISME Journal*,
 994 11, 1386-1399, 2017.
- φ95 Ciais, P., Sabine, C., Bala, G., Bopp, L., Brovkin, V., Canadell, J., Chhabra, A., DeFries, R.,
 996 Galloway, J., Heimann, M., Jones, C., Le Quéré, C., Myneni, R. B., Piao, S., and Thornton, P.:
 997 Carbon and Other Biogeochemical Cycles, in: *Climate Change 2013: The Physical Science
 998 Basis. Contribution of Working Group I to the Fifth Assessment Report of the
 999 Intergovernmental Panel on Climate Change*, edited by: Stocker, T. F., Qin, D., Plattner, G.-
 1000 K., Tignor, M., Allen, S. K., Boschung, J., Nauels, A., Xia, Y., Bex, V., and Midgley, P. M.,
 1001 Cambridge University Press, Cambridge, 467-544, 2013.
- 1φ02 Claire, M. W., Catling, D. C., and Zahnle, K. J.: Biogeochemical modelling of the rise in
 1003 atmospheric oxygen, *Geobiology*, 4, 239-269, 2006.
- 1φ04 Clegg, S. L., and Brimblecombe, P.: The solubility and activity coefficient of oxygen in salt
 1005 solutions and brines, *Geochimica et Cosmochimica Acta*, 54, 3315-3328, 1990.
- 1φ06 Cramer, S. D.: Solubility of methane in brines from 0 to 300°C, *Industrial Engineering and
 1007 Chemistry Process Design and Development*, 23, 533-538, 1984.
- 1φ08 Crespo-Medina, M., Meile, C. D., Hunter, K. S., Diercks, A.-R., Asper, V. L., Orphan, V. J.,
 1009 Tavormina, P. L., Nigro, L. M., Battles, J. J., Chanton, J. P., Shiller, A. M., Joung, D.-J., Amon,
 1010 R. M. W., Bracco, A., Montoya, J. P., Villareal, T. A., Wood, A. M., and Joye, S. B.: The rise
 1011 and fall of methanotrophy following a deepwater oil-well blowout, *Nat Geosci*, 7, 423-427,
 1012 2014.
- 1φ13 Curtis, G. P.: Comparison of approaches for simulating reactive solute transport involving organic
 1014 degradation reactions by multiple terminal electron acceptors, *Computers & Geosciences*, 29,
 1015 319-329, 2003.
- 1φ16 Daines, S. J., and Lenton, T. M.: The effect of widespread early aerobic marine ecosystems on
 1017 methane cycling and the Great Oxidation, *Earth and Planetary Science Letters*, 434, 42-51,
 1018 2016.
- 1φ19 Dale, A. W., Regnier, P., and Van Cappellen, P.: Bioenergetic controls on anaerobic oxidation of
 1020 methane (AOM) in coastal marine sediments: A theoretical analysis, *American Journal of
 1021 Science*, 306, 246-294, 2006.

- 1022 Dale, A. W., Regnier, P., Knab, N. J., Jørgensen, B. B., and Van Cappellen, P.: Anaerobic
1023 oxidation of methane (AOM) in marine sediments from the Skagerrak (Denmark): II. Reaction-
1024 transport modeling, *Geochimica et Cosmochimica Acta*, 72, 2880-2894, 2008.
- 1025 Dickens, G. R., Castillo, M. M., and Walker, J. C. G.: A blast of gas in the latest Paleocene:
1026 simulating first-order effects of massive dissociation of oceanic methane hydrate, *Geology*, 25,
1027 259-262, 1997.
- 1028 Dickens, G. R.: Rethinking the global carbon cycle with a large, dynamic and microbially mediated
1029 gas hydrate capacitor, *Earth and Planetary Science Letters*, 213, 169-183, 2003.
- 1030 Doney, S. C., Lindsay, K., Fung, I., and John, J.: Natural variability in a stable, 1000-yr global
1031 coupled climate-carbon cycle simulation, *Journal of Climate*, 19, 3033-3054, 2006.
- 1032 Duan, Z., Møller, N., Greenberg, J., and Weare, J. H.: The prediction of methane solubility in
1033 natural waters to high ionic strength from 0 to 250°C and from 0 to 1600 bar, *Geochimica et*
1034 *Cosmochimica Acta*, 56, 1451-1460, 1992.
- 1035 Dunfield, P. F., and Conrad, R.: Starvation alters the apparent half-saturation constant for methane
1036 in the Type II methanotroph *Methylocystis* strain LR1, *Appl Environ Microb*, 66, 4136-4138,
1037 2000.
- 1038 Edwards, N. R., and Marsh, R.: Uncertainties due to transport-parameter sensitivity in an efficient
1039 3-D ocean-climate model, *Climate Dynamics*, 24, 415-433, 2005.
- 1040 Egger, M., Rasigraf, O., Sapart, C. J., Jilbert, T., Jetten, M. S. M., Röckmann, T., van der Veen,
1041 C., Banda, N., Kartal, B., Ettwig, K. F., and Slomp, C. P.: Iron-mediated anaerobic oxidation
1042 of methane in brackish coastal sediments, *Environmental Science & Technology*, 49, 277-283,
1043 2015.
- 1044 Egger, M., Riedinger, N., Mogollón, J. M., and Jørgensen, B. B.: Global diffusive fluxes of
1045 methane in marine sediments, *Nat Geosci*, 11, 421-425, 2018.
- 1046 Elliot, S., Maltrud, M., Reagan, M., Moridis, G., and Cameron-Smith, P.: Marine methane cycle
1047 simulations for the period of early global warming, *Journal of Geophysical Research -*
1048 *Biogeosciences*, 116, 10.1029/2010JG001300, 2011.
- 1049 Froelich, P. N., Klinkhammer, G. P., Bender, M. L., Luedtke, N. A., Heath, G. R., Cullen, D., and
1050 Duaphin, P.: Early oxidation of organic matter in pelagic sediments of the eastern equatorial
1051 Atlantic: suboxic diagenesis, *Geochimica et Cosmochimica Acta*, 43, 1075-1090, 1979.
- 1052 Goldblatt, C., Lenton, T. M., and Watson, A. J.: Bistability of atmospheric oxygen and the Great
1053 Oxidation, *Nature*, 443, 683-686, 2006.
- 1054 Griffies, S. M.: The Gent-McWilliams skew flux, *Journal of Physical Oceanography*, 28, 831-841,
1055 1998.

- 1056 Hanson, R. S., and Hanson, T. E.: Methanotrophic bacteria, *Microbiological Reviews*, 60, 439-
1057 471, 1996.
- 1058 Haqq-Misra, J., Domagal-Goldman, S. D., Kasting, P. J., and Kasting, J. F.: A revised, hazy
1059 methane greenhouse for the Archean Earth, *Astrobiology*, 8, 1127-1137, 2008.
- 1060 Haroon, M. F., Hu, S., Shi, Y., Imelfort, M., Keller, J., Hugenholtz, P., Yuan, Z., and Tyson, G.
1061 W.: Anaerobic oxidation of methane coupled to nitrate reduction in a novel archaeal lineage,
1062 *Nature*, 500, 567-570, 2013.
- 1063 Hayes, J. M.: Global methanotrophy at the Archean-Proterozoic transition, in: *Proc. Nobel Symp.*
1064 84, *Early Life on Earth*, edited by: Bengtson, S., Columbia University Press, New York, 220-
1065 236, 1994.
- 1066 Helz, G. R., Bura-Nakic, E., Mikac, N., and Ciglenecki, I.: New model for molybdenum behavior
1067 in euxinic waters, *Chemical Geology*, 284, 323-332, 2011.
- 1068 Hinrichs, K.-U., Hayes, J. M., Sylva, S. P., Brewer, P. G., and DeLong, E. F.: Methane-consuming
1069 archaeobacteria in marine sediments, *Nature*, 398, 802-805, 1999.
- 1070 Hinrichs, K.-U.: Microbial fixation of methane carbon at 2.7 Ga: Was an anaerobic mechanism
1071 possible?, *Geochim. Geophys. Geosyst.*, 3, 1-10, 2002.
- 1072 Hitchcock, D. R., and Lovelock, J. E.: Life detection by atmospheric analysis, *Icarus*, 7, 149-159,
1073 1967.
- 1074 Hoehler, T. M., Alperin, M. J., Albert, D. B., and Martens, C. S.: Field and laboratory studies of
1075 methane oxidation in an anoxic marine sediments: Evidence for a methanogen-sulfate reducer
1076 consortium, *Global Biogeochemical Cycles*, 8, 451-463, 1994.
- 1077 Hoehler, T. M., Alperin, M. J., Albert, D. B., and Martens, C. S.: Apparent minimum free energy
1078 requirements for methanogenic Archaea and sulfate-reducing bacteria in an anoxic marine
1079 sediment, *Fems Microbiol Ecol*, 38, 33-41, 2001.
- 1080 Hoehler, T. M.: Biological energy requirements as quantitative boundary conditions for life in the
1081 subsurface, *Geobiology*, 2, 205-215, 2004.
- 1082 Hunter, S. J., Goldobin, D. S., Haywood, A. M., Ridgwell, A., and Rees, J. G.: Sensitivity of the
1083 global submarine hydrate inventory to scenarios of future climate change, *Earth and Planetary
1084 Science Letters*, 367, 105-115, 2013.
- 1085 Jakobsen, R., and Postma, D.: Redox zoning, rates of sulfate reduction and interactions with Fe-
1086 reduction and methanogenesis in a shallow sandy aquifer, Rømø, Denmark, *Geochimica et
1087 Cosmochimica Acta*, 63, 137-151, 1999.
- 1088 Jayakumar, D. A., Naqvi, S. W. A., Narvekar, P. V., and George, M. D.: Methane in coastal and
1089 offshore waters of the Arabian Sea, *Marine Chemistry*, 74, 1-13, 2001.

- 1090 Jin, Q., and Bethke, C. M.: Predicting the rate of microbial respiration in geochemical
1091 environments, *Geochimica et Cosmochimica Acta*, 69, 1133-1143, 2005.
- 1092 Jin, Q., and Bethke, C. M.: The thermodynamics and kinetics of microbial metabolism, *American
1093 Journal of Science*, 307, 643-677, 2007.
- 1094 Johnson, K. S.: Carbon dioxide hydration and dehydration kinetics in seawater, *Limnology and
1095 Oceanography*, 27, 849-855, 1982.
- 1096 Kasting, J. F., Zahnle, K. J., and Walker, J. C. G.: Photochemistry of methane in the Earth's early
1097 atmosphere, *Precambrian Research*, 20, 121-148, 1983.
- 1098 Kasting, J. F., Pavlov, A. A., and Siefert, J. L.: A coupled ecosystem-climate model for predicting
1099 the methane concentration in the Archean atmosphere, *Origin of life and evolution of the
1100 Biosphere*, 31, 271-285, 2001.
- 1101 Kessler, J. D., Valentine, D. L., Redmond, M. C., Du, M., Chan, E. W., Mendes, S. D., Quiroz, E.
1102 W., Villanueva, C. J., Shusta, S. S., Werra, L. M., Yvon-Lewis, S. A., and Weber, T. C.: A
1103 persistent oxygen anomaly reveals the fate of spilled methane in the deep Gulf of Mexico,
1104 *Science*, 331, 312-315, 2011.
- 1105 Kirschke, S., Bousquet, P., Ciais, P., Saunois, M., Canadell, J. G., Dlugokencky, E. J.,
1106 Bergamaschi, P., Bergmann, D., Blake, D. R., Bruhwiler, L., Cameron-Smith, P., Castaldi, S.,
1107 Chevallier, F., Feng, L., Fraser, A., Heimann, M., Hodson, E. L., Houweling, S., Josse, B.,
1108 Fraser, P. J., Krummel, P. B., Lamarque, J.-F., Langenfelds, R. L., Le Quéré, C., Naik, V.,
1109 O'Doherty, S., Palmer, P. I., Pison, I., Plummer, D., Poulter, B., Prinn, R. G., Rigby, M.,
1110 Ringeval, B., Santini, M., Schmidt, M., Shindell, D. T., Simpson, I. J., Spahni, R., Steele, L.
1111 P., Strode, S. A., Sudo, K., Szopa, S., van der Werf, G. R., Voulgarakis, A., van Weele, M.,
1112 Weiss, R. F., Williams, J. E., and Zeng, G.: Three decades of global methane sources and sinks,
1113 *Nat Geosci*, 6, 813-823, 2013.
- 1114 Kirtland Turner, S., and Ridgwell, A.: Development of a novel empirical framework for
1115 interpreting geological carbon isotope excursions, with implications for the rate of carbon
1116 injection across the PETM, *Earth and Planetary Science Letters*, 435, 1-13, 2016.
- 1117 Kirtland Turner, S.: Constraints on the onset duration of the Paleocene-Eocene Thermal
1118 Maximum, *Philosophical Transactions of the Royal Society A*, 376, 20170082, 2018.
- 1119 Konijnendijk, T. Y. M., Weber, S. L., Tuenter, E., and van Weele, M.: Methane variations on
1120 orbital timescales: a transient modeling experiment, *Climate of the Past*, 7, 635-648, 2011.
- 1121 Krissansen-Totton, J., Garland, R., Irwin, P., and Catling, D. C.: Detectability of biosignatures in
1122 anoxic atmospheres with the *James Webb Space Telescope*: A TRAPPIST-1e cast study, *The
1123 Astrophysical Journal*, 156, 114, 2018.
- 1124 Kuivila, K. M., Murray, J. W., and Devol, A. H.: Methane production, sulfate reduction and
1125 competition for substrates in the sediments of Lake Washington, *Geochimica et Cosmochimica
1126 Acta*, 53, 409-416, 1989.

- 1127 Lamarque, J.-F., Kiehl, J. T., Shields, C. A., Boville, B. A., and Kinnison, D. E.: Modeling the
1128 response to changes in tropospheric methane concentration: Application to the Permian-
1129 Triassic boundary, *Paleoceanography*, 21, 10.1029/2006PA001276, 2006.
- 1130 Lovley, D. R., Dwyer, D. F., and Klug, M. J.: Kinetic analysis of competition between sulfate
1131 reducers and methanogens for hydrogen in sediments, *Appl Environ Microb*, 43, 1373-1379,
1132 1982.
- 1133 Lunt, D. J., Ridgwell, A., Sluijs, A., Zachos, J. C., Hunter, S. J., and Haywood, A.: A model for
1134 orbital pacing of methane hydrate destabilization during the Palaeogene, *Nat Geosci*, 4, 775-
1135 778, 2011.
- 1136 Marsh, R., Müller, S. A., Yool, A., and Edwards, N. R.: Incorporation of the C-GOLDSTEIN
1137 efficient climate model into the GENIE framework: “cb_go_gs” configurations of GENIE,
1138 *Geoscientific Model Development*, 4, 957-992, 2011.
- 1139 Martens, C. S., and Berner, R. A.: Interstitial water chemistry of anoxic Long Island Sound
1140 sediments. 1. Dissolved gases, *Limnology and Oceanography*, 22, 10-25, 1977.
- 1141 McGlynn, S. E., Chadwick, G. L., Kempes, C. P., and Orphan, V. J.: Single cell activity reveals
1142 direct electron transfer in methanotrophic consortia, *Nature*, 526, 531-535, 2015.
- 1143 Melton, J. R., Wania, R., Hodson, E. L., Poulter, B., Ringeval, B., Spahni, R., Bohn, T., Avis, C.
1144 A., Beerling, D. J., Chen, G., Eliseev, A. V., Denisov, S. N., Hopcraft, P. O., Lettenmaier, D.
1145 P., Riley, W. J., Singarayer, J. S., Subin, Z. M., Tian, H., Zürcher, S., Brovkin, V., van
1146 Bodegom, P. M., Kleinen, T., Yu, Z. C., and Kaplan, J. O.: Present state of global wetland
1147 extent and wetland methane modelling: conclusions from a model inter-comparison project
1148 (WETCHIMP), *Biogeosciences*, 10, 753-788, 2013.
- 1149 Meyer, K. M., Ridgwell, A., and Payne, J. L.: The influence of the biological pump on ocean
1150 chemistry: implications for long-term trends in marine redox chemistry, the global carbon
1151 cycle, and marine animal ecosystems, *Geobiology*, 14, 207-219, 2016.
- 1152 Milucka, J., Ferdelman, T. G., Polerecky, L., Franzke, D., Wegener, G., Schmid, M., Lieberwirth,
1153 I., Wagner, M., Widdel, F., and Kuypers, M. M. M.: Zero-valent sulphur is a key intermediate
1154 in marine methane oxidation, *Nature*, 491, 541-546, 2012.
- 1155 Myhre, G., Shindell, D., Breon, F.-M., Collins, W., Fuglestedt, J., Huang, J., Koch, D., Lamarque,
1156 J.-F., Lee, D., Mendoza, B., Nakajima, T., Robock, A., Stephens, G., Takemura, T., and Zhang,
1157 H.: Anthropogenic and natural radiative forcing, in: *Climate Change 2013: The Physical
1158 Science Basis. Contribution of Working Group I to the Fifth Assessment Report of the
1159 Intergovernmental Panel on Climate Change*, edited by: Stocker, T. F., Qin, D., Plattner, G.-
1160 K., Tignor, M., Allen, S. K., Boschung, J., Nauels, A., Xia, Y., Bex, V., and Midgley, P. M.,
1161 Cambridge University Press, Cambridge, 659-740, 2013.
- 1162 Olson, S. L., Kump, L. R., and Kasting, J. F.: Quantifying the areal extent and dissolved oxygen
1163 concentrations of Archean oxygen oases, *Chemical Geology*, 362, 35-43, 2013.

- 1164 Olson, S. L., Reinhard, C. T., and Lyons, T. W.: Limited role for methane in the mid-Proterozoic
1165 greenhouse, *Proceedings of the National Academy of Sciences, USA*, 113, 11447-11452, 2016.
- 1166 Orphan, V. J., House, C. H., Hinrichs, K.-U., McKeegan, K. D., and DeLong, E. F.: Methane-
1167 consuming Archaea revealed by directly coupled isotopic and phylogenetic analysis, *Science*,
1168 293, 484-487, 2001.
- 1169 Ozaki, K., Tajika, E., Hong, P. K., Nakagawa, Y., and Reinhard, C. T.: Effects of primitive
1170 photosynthesis on Earth's early climate system, *Nat Geosci*, 11, 55-59, 2018.
- 1171 Paudel, R., Mahowald, N. M., Hess, P. G. M., Meng, L., and Riley, W. J.: Attribution of changes
1172 in global wetland methane emissions from pre-industrial to present using CLM4.5-BGC,
1173 *Environmental Research Letters*, 11, 034020, 10.1088/1748-9326/11/3/034020, 2016.
- 1174 Pavlov, A. A., Kasting, J. F., and Brown, L. L.: Greenhouse warming by CH₄ in the atmosphere
1175 of early Earth, *Journal of Geophysical Research*, 105, 11981-11990, 2000.
- 1176 Pavlov, A. A., Hurtgen, M. T., Kasting, J. F., and Arthur, M. A.: Methane-rich Proterozoic
1177 atmosphere?, *Geology*, 31, 87-90, 2003.
- 1178 Prather, M. J.: Time scales in atmospheric chemistry: Theory, GWPs for CH₄ and CO, and
1179 runaway growth, *Geophysical Research Letters*, 23, 2597-2600, 1996.
- 1180 Rabouille, C., and Gaillard, J. F.: A coupled model representing the deep-sea organic carbon
1181 mineralization and oxygen consumption in surficial sediments, *J Geophys Res-Oceans*, 96,
1182 2761-2776, 10.1029/90jc02332, 1991.
- 1183 Reeburgh, W. S.: Methane consumption in Cariaco Trench waters and sediments, *Earth and*
1184 *Planetary Science Letters*, 28, 337-344, 1976.
- 1185 Reeburgh, W. S.: Oceanic methane biogeochemistry, *Chemical Reviews*, 107, 486-513, 2007.
- 1186 Regnier, P., Dale, A. W., Arndt, S., LaRowe, D. E., Mogollón, J., and Van Cappellen, P.:
1187 Quantitative analysis of anaerobic oxidation of methane (AOM) in marine sediments: A
1188 modeling perspective, *Earth-Science Reviews*, 106, 105-130, 2011.
- 1189 Reinhard, C. T., Planavsky, N. J., Olson, S. L., Lyons, T. W., and Erwin, D. H.: Earth's oxygen
1190 cycle and the evolution of animal life, *Proceedings of the National Academy of Sciences, USA*,
1191 113, 8933-8938, 2016.
- 1192 Reinhard, C. T., Olson, S. L., Schwieterman, E. W., and Lyons, T. W.: False negatives for remote
1193 life detection on ocean-bearing planets: Lessons from the early Earth, *Astrobiology*, 17,
1194 doi:10.1089/ast.2016.1598, 2017.
- 1195 Ridgwell, A.: Glacial-interglacial perturbations in the global carbon cycle, PhD, University of East
1196 Anglia, Norwich, UK, 2001.

- 1197 Ridgwell, A., Hargreaves, J. C., Edwards, N. R., Annan, J. D., Lenton, T. M., Marsh, R., Yool, A.,
1198 and Watson, A.: Marine geochemical data assimilation in an efficient Earth System Model of
1199 global biogeochemical cycling, *Biogeosciences*, 4, 87-104, 2007.
- 1200 Ridgwell, A. J., Marshall, S. J., and Gregson, K.: Consumption of atmospheric methane by soils:
1201 A process-based model, *Global Biogeochemical Cycles*, 13, 59-70, 1999.
- 1202 Sagan, C., and Mullen, G.: Earth and Mars: Evolution of atmospheres and surface temperatures,
1203 *Science*, 177, 52-56, 1972.
- 1204 Sagan, C., Thompson, W. R., Carlson, R., Gurnett, D., and Hord, C.: A search for life on Earth
1205 from the Galileo spacecraft, *Nature*, 365, 715-721, 1993.
- 1206 Sansone, F. J., Popp, B. N., Gasc, A., Graham, A. W., and Rust, T. M.: Highly elevated methane
1207 in the eastern tropical North Pacific and associated isotopically enriched fluxes to the
1208 atmosphere, *Geophysical Research Letters*, 28, 4567-4570, 2001.
- 1209 Schink, B.: Energetics of syntrophic cooperation in methanogenic degradation, *Microbiology and
1210 Molecular Biology Reviews*, 61, 262-280, 1997.
- 1211 Schmidt, G. A., and Shindell, D. T.: Atmospheric composition, radiative forcing, and climate
1212 change as a consequence of a massive methane release from gas hydrates, *Paleoceanography*,
1213 18, 1004, 10.1029/2002PA000757, 2003.
- 1214 Schrag, D. P., Berner, R. A., Hoffman, P. F., and Halverson, G. P.: On the initiation of a snowball
1215 Earth, *Geochem. Geophys. Geosyst.*, 3, 10.1029/2001GC000219 (Available at [http://www.g-
1216 cubed.org](http://www.g-cubed.org)), 2002.
- 1217 Scranton, M. I., and Brewer, P. G.: Consumption of dissolved methane in the deep ocean,
1218 *Limnology and Oceanography*, 23, 1207-1213, 1978.
- 1219 Shindell, D. T., Pechony, O., Voulgarakis, A., Faluvegi, G., Nazarenko, L., Lamarque, J.-F.,
1220 Bowman, K., Milly, G., Kovari, B., Ruedy, R., and Schmidt, G. A.: Interactive ozone and
1221 methane chemistry in GISS-E2 historical and future climate simulations, *Atmospheric
1222 Chemistry and Physics*, 13, 2653-2689, 2013.
- 1223 Sivan, O., Adler, M., Pearson, A., Gelman, F., Bar-Or, I., John, S. G., and Eckert, W.: Geochemical
1224 evidence for iron-mediated anaerobic oxidation of methane, *Limnology and Oceanography*,
1225 56, 1536-1544, 2011.
- 1226 Stoessell, R. K., and Byrne, P. A.: Salting-out of methane in single-salt solutions at 25°C and below
1227 800 psia, *Geochimica et Cosmochimica Acta*, 46, 1327-1332, 1982.
- 1228 Thamdrup, B., Steinsdóttir, H. G. R., Bertagnolli, A. D., Padilla, C. C., Patin, N. V., Garcia-
1229 Robledo, E., Bristow, L. A., and Stewart, F. J.: Anaerobic methane oxidation is an important
1230 sink for methane in the ocean's largest oxygen minimum zone, *Limnology and Oceanography*,
1231 10.1002/lno.11235, 2019.

- 1232 Thompson, A. M., and Cicerone, R. J.: Possible perturbations to atmospheric CO, CH₄, and OH,
1233 *Journal of Geophysical Research*, 91, 10853-10864, 1986.
- 1234 Ueno, Y., Yamada, K., Yoshida, N., Maruyama, S., and Isozaki, Y.: Evidence from fluid inclusions
1235 for microbial methanogenesis in the early Archaean era, *Nature*, 440, 516-519, 2006.
- 1236 Ulfsbo, A., Abbas, Z., and Turner, D. R.: Activity coefficients of a simplified seawater electrolyte
1237 at varying salinity (5-40) and temperature (0 and 25°C) using Monte Carlo simulations, *Marine*
1238 *Chemistry*, 171, 78-86, 2015.
- 1239 Valentine, D. L.: Emerging topics in marine methane biogeochemistry, *Annual Review of Marine*
1240 *Science*, 3, 147-171, 2011.
- 1241 van Bodegom, P., Stams, F., Liesbeth, M., Boeke, S., and Leffelaar, P.: Methane oxidation and the
1242 competition for oxygen in the rice rhizosphere, *Appl Environ Microb*, 67, 3586-3597, 2001.
- 1243 Van Cappellen, P., Gaillard, J.-F., and Rabouille, C.: Biogeochemical transformations in
1244 sediments: Kinetic models of early diagenesis, in: *Interactions of C, N, P and S*
1245 *Biogeochemical Cycles and Global Change*, Springer, 401-445, 1993.
- 1246 Walter, B. P., and Heimann, M.: A process-based, climate-sensitive model to derive methane
1247 emissions from natural wetlands: Application to five wetland sites, sensitivity to model
1248 parameters, and climate, *Global Biogeochemical Cycles*, 14, 745-765, 2000.
- 1249 Wania, R., Ross, I., and Prentice, I. C.: Implementation and evaluation of a new methane model
1250 within a dynamic global vegetation model: LPJ_WHyMe v1.3.1, *Geoscientific Model*
1251 *Development*, 3, 565-584, 2010.
- 1252 Weber, T., Wiseman, N. A., and Kock, A.: Global ocean methane emissions dominated by shallow
1253 coastal waters, *Nature Communications*, 10, 4584, 10.1038/s41467-019-12541-7, 2019.
- 1254 Zeebe, R. E., Zachos, J. C., and Dickens, G. R.: Carbon dioxide forcing alone insufficient to
1255 explain Palaeocene-Eocene Thermal Maximum warming, *Nat Geosci*, 2, 576-580, 2009.
- 1256 Zeebe, R. E.: What caused the long duration of the Paleocene-Eocene Thermal Maximum?,
1257 *Paleoceanography*, 28, 1-13, 10.1002/palo.20039, 2013.
- 1258